This is the peer reviewed version of the following article: Paillassa, J., Pepin, S., Ethier, G., Lamarque, L. J., & Maire, V. Carboxylation capacity is the main limitation of carbon assimilation in High Arctic shrubs. Plant, Cell & Environment. , which has been published in final form at https://doi.org/10.1111/pce.15097. This article may be used for non-commercial purposes in accordance with Wiley Terms and Conditions for Use of Self-Archived Versions. This article may not be enhanced, enriched or otherwise transformed into a derivative work, without express permission from Wiley or by statutory rights under applicable legislation. Copyright notices must not be removed, obscured or modified. The article must be linked to Wiley's version of record on Wiley Online Library and any embedding, framing or otherwise making available the article or pages thereof by third parties from platforms, services and websites other than Wiley Online Library are prohibited.

Carboxylation capacity is the main limitation of carbon assimilation in High Arctic shrubs

Jennifer Paillassa[1,2,3,4], Steeve Pepin[4], Gilbert Ethier[5], Laurent J. Lamarque[1,2,3], Vincent Maire[1,2,3]

[1]Département des Sciences de l'environnement, Université du Québec à Trois-Rivières, Trois-Rivières, QC, Canada;

[2]Chaire en Écologie Fonctionnelle Arctique, Centre d'études nordiques, Université du Québec à Trois-Rivières, Trois Rivières, Qc, G9A 5H7, Canada;

[3]Centre d'études nordiques, Université Laval, Québec, QC, Canada;

[4]Département des sols et de génie agroalimentaire, Université Laval, Québec, QC, G1V 0A6, Canada

[5]Département de phytologie, Université Laval, Québec, QC, G1V 0A6, Canada

Correspondence: steeve.pepin@fsaa.ulaval.ca; gilbert.ethier@fsaa.ulaval.ca; vmaire24@gmail.com

Keywords: High Arctic tundra, mesophyll conductance, stomatal conductance, carboxylation capacity, *Salix arctica*, *Salix reticulata*, *Salix richardsonii*, shrubification, leaf nitrogen use efficiency.

Manuscript length:

Abstract: 199; Introduction: 1276; Material & Methods: 1946; Results: 871; Discussion: 2020; All (including ref): 8704; References: 2453; Figures: 6; Tables: 3.

Abstract

Increases in shrub height, biomass and canopy cover are key whole-plant features of warming-induced vegetation change in tundra. In this study, we investigated leaf functional traits underlying the photosynthetic capacity of Arctic shrub species, particularly its main limiting processes such as mesophyll conductance. In this nutrient-limited ecosystem, we expect leaf nitrogen concentration to be the main limiting factor for photosynthesis.

We measured the net photosynthetic rate at saturated light (A_{sat}) in three Salix species throughout a glacial valley on Bylot Island in High-Arctic tundra and used a causal approach to test relationships between leaf stomatal and mesophyll conductances (g_{sc}, g_m), carboxylation capacity (Vc_{max}), nitrogen and phosphorus concentration (N_{area}, P_{area}) and leaf mass ratio (LMA).

Arctic Salix species showed no difference in A_{sat} compared to a global dataset, while being characterized by higher N_{area}, P_{area} and LMA. Within and between species, A_{sat} increased with increasing N_{area} and P_{area} and decreasing LMA. Vc_{max}, g_{sc} and g_m independently increased A_{sat}, with Vc_{max} as its main limitation. We highlighted a nitrogen-influenced pathway for increasing photosynthesis in the two prostrate mesic habitat species. In contrast, the erect wetland habitat *S. richardsonii* mainly increased A_{sat} with increasing g_{sc}.

Overall, our study revealed high photosynthetic capacities of Arctic Salix species but contrasting regulatory pathways that may influence shrub ability to respond to environmental changes in High Arctic tundra.

Introduction

The Arctic has warmed at a rate of 0.73 °C decade^{-1} over the last forty years (Rantanen et al., 2022), leading to major vegetation changes across the Arctic tundra biome. These changes have been characterized by the faster growth, increased height, and northward expansion of shrub species (Forbes et al., 2010; Tape et al., 2006). The 'shrubification' phenomenon has been studied extensively in multiple ways (Vowles & Björk, 2019), notably regarding its impacts on species composition and functional diversity of plant communities (Bjorkman et al., 2018), plant-soil interactions (Street et al., 2020), soil properties (Lamarque et al. 2023) and regional climate (Bonfils et al., 2012). Comparatively, few studies have examined the determinants of photosynthetic capacity in Arctic shrubs. Indeed, the latter has only been measured in a handful of species (*Betula nana, Salix arctica, S. glauca, S. polaris, S. pulchra*) across eight sites to date (Bredahl et al., 2004; Johnson & Tieszen, 1976; Chapin & Shaver, 1989; Fletcher et al., 2012; Baddeley et al., 1994; Muraoka et al., 2002), and we do not yet know the extent to which the underlying diffusional (stomatal and mesophyll) and biochemical (e.g. maximal ribulose-1,5-bisphosphate carboxylation rate, Vc_{max}) components limit photosynthetic CO_2 assimilation in the Arctic. However, a better characterization of CO_2 uptake and its limitations among Arctic shrubs would bring new insights on the traits and species strategies that are associated to shrubification. This is important as photosynthetic capacity and particularly, its relationship to leaf nitrogen content are two of the most sensitive parameters of terrestrial biosphere models (Kattge et al. 2009).

Our current understanding of the variation in leaf photosynthetic capacity across species follows the global trend established among leaf functional traits, the so-called leaf economic spectrum (Wright et al., 2004; Diaz et al., 2016), which runs from species with short-lived foliage and fast metabolism to species with slow return on carbon and nutrient investments. The latter functional group is expected to be found in the cold and nutrient-poor environment of low productive Arctic tundra and is notably characterized by species with thick leaves and low nutrient content having low photosynthetic capacity. Although the leaf economic spectrum has been formulated predominantly from data acquired in temperate and tropical environments (Kattge et al., 2011), recent investigations within the tundra biome showed that it tends to hold true in the cold extremes of the planet (Thomas et al., 2020). Yet, Reich & Oleskyn (2004) showed that some Arctic species can reach very high level of leaf nitrogen (N) and phosphorus (P) concentration, while Rogers et al. (2017) demonstrated in seven species that such high N level allowed photosynthetic capacities measured in the tundra to be two- to five-fold higher

than the values used to parameterize current Earth system models. Thus, it is still relatively unclear how well the variation in leaf chemical and biometric traits found among Arctic species reflects their photosynthetic capacity.

Variation in the photosynthetic capacity of leaves versus nutrient content defines their photosynthetic nutrient-use efficiency, which encompasses the nutrient allocation to the photosynthetic apparatus and/or specific activity of photosynthetic enzymes as opposed to investment into structural/protective compounds notably found in cell walls (Onoda et al., 2017). In general, within-species variation of photosynthetic capacity is related to leaf nitrogen content (Hikosaka, 2010 but see Kong et al., 2022). In cold environments, an increase in leaf N both within and across species likely reflects a physiological acclimation (physiological response) and adaptation (evolutionary response) process that compensates for the temperature depression of the Rubisco-catalyzed CO_2 carboxylation rate (Baddeley et al., 1994; Körner, 1999). As such, increasing N in leaf tissue is expected to favor the production of N-rich proteins like Rubisco and lead to higher CO_2 carboxylation capacity (Hikoska, 2010). In the cold and low nitrogen availability tundra, increasing N availability through temperature and fertilization effectively led to higher photosynthetic capacity in several (but not all) Arctic tundra species (Oechel et al., 1994; Chapin & Shaver, 1996) (path 2, Fig. 1). However, leaf N is not necessarily capitalized as functional photosynthetic enzymes, as observed under phosphorus deficiency (Walker et al., 2014; Luo et al., 2021). Nitrogen can be used in the production of photoprotective molecules against daylong light, such as carotenoids (Fernandez-Marin et al., 2020) and in cell wall proteins (Onoda et al., 2017). In addition, it has been suggested that tundra productivity is more related with plant sink capacity (ontogenic development) rather than photosynthetic (i.e., source) capacity (Körner, 2015). In such cases, leaf N may not constrain the photosynthetic capacity (Bliss, 1972; Chapin et al., 1995). Overall, it remains unclear if within Arctic tundra species increasing leaf N content leads to an increase in photosynthetic capacity.

In cold environments, photosynthetic limitation may be dominated by diffusive processes lowering the chloroplastic CO_2 concentration (C_c) per unit Rubisco, a condition that may have contributed to the adaptive increase in Rubisco's specificity factor for its CO_2 substrate as opposed to O_2 in tundra species (Galmès et al., 2016 & 2019; Sàez et al., 2017). In Antarctica mesophyll conductance (g_m) represented the major photosynthetic limitation for the two known vascular species *Deschampsia antarctica* and *Colobanthus quitensis* (Saez et al., 2018; path 3, Fig. 1). Although lower temperature enhances CO_2 solubility and favors the liquid phase component of g_m, CO_2 transfer through cellular membranes may overwhelmingly be

113 reduced under such condition (Evans & von Caemmerer 2013) (path 3, Fig. 1). In the Arctic,
114 the high leaf mass per unit area (LMA) that permits long leaf lifespans (Chapin et al., 1995) is
115 commonly associated with thicker cell walls, greater cell wall mass allocation per unit leaf area,
116 and a thicker and denser leaf mesophyll, all leaf anatomical characteristics that are known to
117 lower g_m (Théroux-Rancourt et al., 2017; Onoda et al., 2017) (path 10, Fig. 1). Cold
118 environments are also associated with high water viscosity, which can strongly reduce plant
119 hydraulic conductivity and, ultimately, establishes stomatal conductance (g_s) as the main
120 limiting factor for photosynthetic capacity (Galmès et al., 2016) (path 1, Fig. 1).

121 Our study aims to elucidate whether the photosynthetic capacity of shrub species is
122 particularly limited in High-Arctic tundra, whether mesophyll conductance is the main
123 photosynthetic limitation as in Antarctica, and finally whether and how this may differ between
124 species. We evaluated the diffusive vs. biochemical limitations of photosynthesis in three Salix
125 shrub species that co-occur in a glacial valley in Bylot Island (Nunavut, Canada): prostrate
126 *Salix arctica* and *S. reticulata*, and *S. richardsonii* that is the only erect species of the island.
127 Specifically, we aimed to:

128 (i) Determine if Arctic Salix species are particularly characterized by low values
129 of light-saturated photosynthesis rate (A_{sat}), low N_{area} and P_{area} despite high
130 LMA, as it would be expected in this biome from the leaf economic spectrum
131 (Wright et al., 2005). From this framework, we also expect that within-species
132 variation of A_{sat} is positively related to N_{area} and P_{area} but negatively related to
133 LMA.

134 (ii) Disentangle the influence of diffusional and biochemical processes on A_{sat}.
135 While g_{sc} (stomatal conductance to CO_2), g_m (mesophyll conductance) and
136 photosynthetic capacity (i.e., Vc_{max}) should be coordinated, we expect the
137 allocation of N towards Vc_{max} to dominate the limitation of A_{sat} in the low
138 nitrogen availability Arctic tundra.

139 (iii) Disentangle the influence of leaf chemical and biometric traits on A_{sat} and
140 diffusive processes among species. While we expect a key role of N_{area} on Vc_{max}
141 for the prostrate Salix species, we also expect a different regulatory pathway in
142 *S. richardsonii,* whose taller stature may constrain the transport of cold and
143 dense water to leaves (Fig.1).

Materials and methods

Site & Species selection

The study was conducted in the Qarlikturvik glacial valley of Bylot Island, Nunavut, Canada, in the High Arctic (73°09'N, 79°57'W). The High Arctic is a region within the Arctic Circle that experiences extreme cold temperatures, permafrost, limited precipitation, and short growing seasons. This area is typically located north of the tree line and includes parts of northern Canada, Greenland, and the northernmost islands of Norway and Russia. In contrast to the Low Artic, the High-Arctic is devoid of trees; however, woody and shrub species are still present and characterized by small and prostrate stature (Myer-Smith et al. 2011).

The average environmental conditions in the Qarlikturvik valley are as follows: altitude, 20 to 400 m; growing season solar radiation, ca. 221 W m^{-2}; annual temperature, -14.4°C; growing season temperature, 4.7°C; snow, ~ 8 months $year^{-1}$; permanent permafrost; precipitation 77.5 mm during the growing season (Domine et al., 2021). The Qarlikturvik Valley is in the southwestern plain of the island and is crossed at its center by a proglacial river. The valley is about 18 km long, has a terrace about 5 km wide at the bottom and is bordered by plateaus up to 500 m in altitude (Godin & Fortier, 2012). It represents a typical glacial valley geosystem with depositional environments, which includes alluvial, eolian, glaciofluvial, morainic, colluvial and marine sediments (Coulombes et al., 2021). The ground is permanently frozen, with a thaw front depth varying from a few centimeters up to 80 cm (Deschamps et al., 2022). A low-centered polygon landscape characterizes the valley with two baseline vegetation types. Wetlands represent 23% of the valley area and are dominated by sedges (*Carex aquatilis*, *Eriophorum angustifolium*, *E. scheuzerii*), grasses (*Dupontia fischeri*) and mosses (*Calliergon giganteum, Drepanocladus* spp.) (Gauthier et al., 1995). Mesic environments occur on polygonal rims, degraded and high centered polygons and hummocky tundra, and support a more diverse group of species composed of *Salix spp.*, *Vaccinium uliginosum*, *Arctagrostis latifolia*, *Poa arctica* and the dominant moss *Aulacomnium spp.* (Perreault et al., 2016).

Salix arctica and *S. reticulata* are prostrate species whose stature rarely exceeds 15 cm with elliptic to oblong leaves ranging from 1 to 10 cm^2 in area. *S. arctica* leaves are more hypostomatous and pilose, while *S. reticulata* are more amphistomatous and glabrescent with venation deeply impressed on the adaxial surface. Both species typically dominate the mesic environments of the Qarlikturvik valley. *S. richardsonii* is the only erect species in the prostrated tundra of Bylot Island, which is located at its northern edge of its distribution range. There, it reaches up to 1 m in height with lanceolate and pilose (and hemiamphistomatous)

leaves and is mainly found along small streams and alluvial fans that cross the valley from the surrounding plateaus to the glacial river (Duclos, 2002; Tremblay, 2017).

Experimental design and plant sampling

We selected twenty-nine sites in July 2019 to represent the diversity of ecosystems encountered in the Qarlikturvik valley, near the glacier to the ocean and from the wetlands along the river glacier up to the mesic plateau. Across sites, topsoil (0-10 cm) varied from 4.6 to 7.8 in pH, from 9.6 to 74.6% in silt percentage and from 0.3 to 28.2% in soil organic matter content, whereas thaw front depth varied from 20.5 to 71.5 cm (recorded between 10-15 August). Microclimate was less variable across sites, ranging from 5.8°C to 6.9°C in mean temperature and from 0.14 to 0.20 kPa in air vapour pressure deficit (VPD) over the June-July-August growing period. At each site, we sampled the three Salix species, *S. arctica*, *S. reticulata*, *S. richardsonii*, whenever possible (23 of 29 sites presented the three species, with *S. reticulata* and *S. richardsonii* absent in one and five sites, respectively). For each species at each site, stems of three different individuals were dug up down to roots then placed in their entirety in an opaque plastic bag to encourage stomatal closure and limit water loss by transpiration during transport to the main camp. There, the individual branches were cut under water and left in the dark for 24 hours before beginning the gas exchange measurements.

Leaf gas exchange measurements

From July 1st to July 20th, we performed instantaneous gas exchange measurements under saturating light on one top-leaf per individual and two individuals per species, and per site~~s~~ (N = 162; n = 58 for *S. arctica*, n = 56 for *S. reticulata*, n = 48 for *S. richardsonii*). Two cross-calibrated portable photosynthesis systems, one LI-6400XT and one LI-6800 (LI-COR Inc., Lincoln, NE, USA), each fitted with a 2 cm^2 window Leaf Chamber Fluorometer to accommodate the small size of Arctic Salix leaves, were used to perform coupled leaf gas exchange and chlorophyll fluorescence measurements. We set the leaf chamber air relative humidity at 60% and leaf temperature (T_{leaf}) at 10ºC. This temperature approximated the average growth condition (mean daily temperature in July = 7.7°C, varying between -1.5 to 22.3°C in the 2013-2019 period (Domine et al., 2021) and prevented condensation issues within the chamber. One hour before measurement, plants were placed under a LED lamp (YGROW S1500 Grow Light) and exposed to a photosynthetic photon flux density (PPFD) of 1000 µmol m^{-2} s^{-1}. At this level, photosynthesis is considered as light-saturated for Arctic tundra shrub species (Leffler & Welker 2013; Mbufong et al., 2014; Walther et al., 2018) as circumarctic vegetation is adapted to relatively low light intensities (Mooney & Billings, 1961). After

clamping the leaf into the chamber, we waited for steady state conditions (typically 10 min) before recording A_{sat} and g_{sc} as well as steady-state (F_s) and maximal (F_m', determined using a 800 ms rectangular flash of PPFD = 8000 µmol m^{-2} s^{-1}) chlorophyll fluorescence under ambient (409 ppm) leaf chamber CO_2 concentration (C_a), then repeated the measurements under 10 different leaf chamber CO_2 concentrations (resulting from setting the instrument's Reference CO_2 from 50 to 900 ppm) to generate a CO_2 response (A-C_i) curve (see Fig. S1). At the end of the A-C_i curve, the leaf chamber CO_2 concentration was set back to the ambient atmospheric level (409 ppm) and the chamber incident PPFD reduced to 100 µmol m^{-2} s^{-1} to acclimate the leaf to light-limiting conditions before performing light response (A-Q) curve measurements under decreasing PPFD (from 100 to 40 µmol m^{-2} s^{-1}), keeping the calculated leaf internal CO_2 concentration (C_i) constant throughout to subsequently estimate non-photorespiratory leaf respiration in the light (R_{day}) using the "Kok effect" method (Kirschbaum & Farquhar 1987). For comparison, we also recorded the leaf respiration rate in the dark (R_{dark}) following 10 minutes stabilization in darkness.

Estimation of g_m, Vc_{max} and J

We used the A-C_i curve fitting method of Ethier & Livingston (2004) in combination with the chlorophyll fluorescence-based estimation of the electron transport rate (*J*) under RuBP regeneration-limited conditions to estimate g_m and Vc_{max} by solving $A_{sat} = \min\{A_c, A_j\}$ where A_c (RuBP-saturated net photosynthetic rate) and A_j (RuBP regeneration-limited net photosynthetic rate) are respectively given by:

$$A_c = \frac{-b+\sqrt{b^2+4ac}}{2a}$$

$$a = -1/g_m$$

$$b = \left(Vc_{max} - R_{day}\right)/g_m + C_i + K_C\,(1 + O/K_O)$$

$$c = -\left(Vc_{max} - R_{day}\right)(C_i - \Gamma) \qquad \text{Eqn 1a}$$

and

$$A_j = \frac{-b+\sqrt{b^2+4ac}}{2a}$$

$$a = -1/g_m$$

$$b = \left(s \cdot \Phi_{PSII} \cdot PPFD/4 - R_{day}\right)/g_m + C_i + 2\,\Gamma^*$$

$$c = R_{day}(C_i + 2\,\Gamma^*) - (s \cdot \Phi_{PSII} \cdot PPFD/4)(C_i - \Gamma^*) \qquad \text{Eqn 1b.}$$

The parameters *s* (an empirical factor relating the chlorophyll fluorescence-based estimation of the photochemical efficiency of photosystem II ($\Phi_{PSII} = (F_m'-F_s)/F_m'$) to *J* (i.e. *J* =

241 $s \cdot \Phi_{PSII} \cdot PPFD$) by accounting for leaf absorbance, partitioning of the absorbed quanta between
242 photosystems I and II, and non-photosynthetic electron transport towards alternate sinks) and
243 Γ (leaf CO_2 compensation point where $A_{sat} = 0$) were solved together with g_m and Vc_{max}, with
244 average (± SD, n = 162) values of 0.38 (± 0.07) and 49 (± 16) ppm for s and Γ, respectively, at
245 T_{leaf} = 10˚C. The assumed 10˚C values of the Rubisco kinetic constants Γ^* (chloroplastic CO_2
246 compensation point), K_c and K_o (Michaelis–Menten constants for RuBP carboxylation and
247 oxygenation, respectively) were taken from Bernacchi et al. (2002). Then, we solved the model
248 for the theoretical case where $A_c = A_j$, that is the net photosynthetic rate ($A_{transition}$) achieved
249 when Vc_{max} limitation is in perfect balance with electron transport rate (J) limitation and
250 compared the later with the measured A_{sat} determined at ambient CO_2 concentration (C_a = 409
251 ppm). As Figure S2b shows, A_{sat} correlated tightly with $A_{transition}$ following essentially a 1:1
252 relationship, which we took as sufficient ground for assuming a near co-limited state for A_{sat}
253 and to carry out our subsequent analyses based on Vc_{max} limitation (see also Figs. S1,S2a and
254 Table S1).

255 **Biometric and chemical traits**

256 Immediately after the gas exchange measurements, we measured the leaf area using a digital
257 camera and weighed the leaf fresh, then weighted its dry mass after 48h oven drying at 70°C.
258 The N and P concentration of finely ground dry leaf material was determined using respectively
259 a Thermal Conversion Elemental Analyzer - Isotope Ratio Mass Spectrometer (Agilent
260 technology, Santa Clara, CA, USA) and an Inductively Coupled Plasma Optical Emission
261 Spectroscopy spectrometer (Plasma Model 40, PerkinElmer, Waltham, MA, USA).

262 **Statistical analyses**

263 All analyses were performed on R statistical software (v.4.3.1; R Foundation for Statistical
264 Computing, Vienna, Austria).

265 *Assessing where Arctic Salix species stand along the leaf economics spectrum (objective 1) –*
266 Leaf trait values measured in Salix species were compared to the global trait distributions from
267 the Globamax database (Maire et al., 2015) in which we only selected C3 photosynthesis type
268 (n = 2409). First, we tested whether Arctic Salix displayed a more conservative strategy
269 compared to species from other biomes. We used a Welch t-test, considering that the variance
270 between the two groups (i.e. Salix vs Globamax) were not equalled. Second, we tested whether
271 A_{sat} covaried positively with leaf N_{area} and P_{area} and negatively with LMA, using a mixed
272 regression model (lme4 package) with a Gaussian distribution family. We considered site and

273 sampling date as random factors to focus primarily on trait co-variations that were not related
274 to ontogeny (Muraoka et al., 2002; Bredahl et al., 2004) and between-site environmental
275 differences. We tested whether species differed in the response of A_{sat} to economic traits by
276 selecting the model that minimizes the Aikaike criterion (AICC) among the alternative models
277 that considered all species*trait pair interactions.

278 *Disentangling the influence of diffusional and biochemical processes on A_{sat} (objective 2)* – We
279 used two different approaches. The first approach used the equations described in Grassi and
280 Magnani (2005) to calculate the relative photosynthetic limitations imposed by the stomatal
281 (L_s), mesophyll (L_m), and biochemical (i.e. carboxylation) (L_b) resistances operating in series.
282 Using a t-test model with equal variances, we tested whether L_s, L_m, and L_b differed among
283 species. However, this approach is not directly based on A_{sat} variation, but on the relative
284 decrease of A_{sat} associated with the successive CO_2 drawdowns leading to the final
285 carboxylation of RuBP. In addition, this approach does not consider the potential
286 interdependency of the reaction-diffusion processes making up the overall photosynthetic
287 limitation. To evaluate the potential influence stomatal and mesophyll CO_2 diffusion processes
288 may have on biochemical photosynthetic capacity, we used a second approach consisting in a
289 standardized and mixed regression model. For each species, we considered g_{sc}, g_m, Vc_{max} and
290 the three ways interaction as fixed factors, as well as site and sampling date as random factors.
291 We used a Gaussian family to represent A_{sat} distribution. The values of g_{sc}, g_m, Vc_{max} were
292 scaled (scale function) to estimate their respective importance.

293 *Disentangling the influence of leaf chemical and biometric traits (N_{area}, P_{area}, LMA) on the*
294 *photosynthetic capacity (A_{sat}) and processes (Vc_{max}, g_{sc}, g_m) (objective 3)* – We used a series of
295 generalized mixed regression models. We additionally tested if the three Salix species differ in
296 their respective leaf trait relationships considering either the additive or interactive effect of
297 species in the model. We used a gamma family distribution for Vc_{max} and g_m and a Gaussian
298 distribution for g_{sc}. Finally, we used a series of mixed regression structured in path analyses
299 ('lme4' and 'piecewiseSEM' packages) to explore how variation in A_{sat} can best be understood
300 as driven by both direct and indirect effects between photosynthetic processes (g_{sc}, g_m, Vc_{max})
301 and leaf biometric and chemistry (N_{area}, P_{area}, LMA). We considered site and sampling date as
302 random factors. We built our initial path model based on established relationships in the
303 literature (see Fig. 1). We selected a common model for the three species that was the least
304 different from the observations (P-value > 0) and applied it separately to each species. Finally,
305 we tested whether differences in photosynthetic pathway among species was consistent with

photosynthetic nitrogen-use efficiency (PNUE = A_{sat}/N_{area}) and instantaneous water use efficiency (WUE = $A_{sat}/(1.6 \cdot g_{sc})$). We used generalized mixed regression models considering site and sampling date as random factors.

Results

Position of Arctic *Salix* species along the leaf economic spectrum

The distribution of A_{sat} values of Arctic Salix species from Bylot Island (median = 10.09, mean = 10.06 ± 0.28 µmol m^{-2} s^{-1} at leaf temperature of 10°C) was comparable to the one observed at the global scale (median = 9.60, mean = 10.60 ± 0.13 µmol m^{-2} s^{-1}, Welch-test: P-value = 0.48 at average leaf temperature of 25.5°C), except that it did not include the high value tail (> 20 µmol m^{-2} s^{-1}; Fig. 2). Yet, differences arose in trait value distributions between *Salix* and Globamax for all the other traits measured (Fig. 2). LMA and PNUE were higher and lower, respectively, when compared with Globamax values (LMA = 137.2 g m^{-2}, PNUE = 2.89 µmol gN^{-1} s^{-1} for Bylot *vs* LMA = 118.025 g m^{-2}, PNUE = 5.72 µmol gN^{-1} s^{-1} for Globamax). Higher values of N_{area} and P_{area} as well as leaf intercellular CO_2 concentration, C_i, particularly characterized Salix species (N_{area} = 3.61 g m^{-2}, P_{area} = 0.353 g m^{-2}, C_i = 350.8 ppm for Bylot *vs* N_{area} = 1.94 g m^{-2}, P_{area} = 0.126 g m^{-2}, C_i = 257.3 ppm for Globamax). Finally, Vc_{max}, g_{sc} and g_m at growth temperature showed significantly lower values for Salix species in comparison with the Globamax distribution (Vc_{max} = 28.15 µmol m^{-2} s^{-1}, g_{sc} = 112.63 mmol m^{-2} s^{-1} and g_m = 116.36 mmol m^{-2} s^{-1} for Bylot vs Vc_{max} = 74.04, g_{sc} = 171.5, g_m = 194.36 for Globamax).

In our study, A_{sat} was positively related to N_{area} and P_{area}, and negatively related to LMA (Figs. 3a,b,c; Table 1). Across species, *S. richardsonii* showed a lower increase in A_{sat} for a given increase in N_{area} compared with *S. arctica* and *S. reticulata* ($(p(Sp*N_{area}) < 0.01)$, Fig. 3a). The relationship between A_{sat} and N_{mass} showed a lower determination coefficient in comparison with an expression on area unit basis (r_m^2 =0.12 vs r_m^2 = 0.27, respectively; data not shown). A_{sat} and PNUE decreased significantly with increasing LMA, the slope of the relationship being similar across species (Table 1, Fig. 3c,e). P_{area} tended to increase A_{sat} and PNUE, but the effect was not significant.

Influence of diffusional and biochemical processes (g_{sc}, g_m, Vc_{max}) on A_{sat}

At ambient CO_2 concentrations, photosynthesis in the three Salix species was mainly Rubisco limited (Fig. 4). There was no significant difference among species and overall g_{sc}, g_m, and Vc_{max} contributed to 21.9%, 19.6%, and 58.5% of A_{sat} limitation, respectively.

The processes, g_{sc}, g_m and Vc_{max}, contributed positively and independently to A_{sat}

338 variation (Table 2, Fig. 5). When considering multiple interactions between photosynthetic
339 processes, the positive effect of Vc_{max} on A_{sat} increased as g_{sc} increased (Figs. 5a-c), whereas
340 the positive effect of g_m on A_{sat} increased as g_{sc} decreased ($p(Vc_{max}*g_{sc}) < 0.01$ and $p(g_{sc}*g_m) <$
341 0.01, respectively, Table 2, Fig. 5). Moreover, the relative importance of photosynthetic
342 processes differed among species, with Vc_{max} being the main determinant of A_{sat} in *S. arctica*
343 and *S. reticulata*, while A_{sat} in *S. richardsonii* was primarily g_{sc} and g_m dependent.

344 **Direct and indirect effects of leaf biometric and chemistry on photosynthesis**

345 Carboxylation capacity (Vc_{max}) and g_m were positively and significantly related to N_{area} (Table
346 3, Figs. S3b,c), and negatively and significantly related to LMA (Table 3, Figs. S3h,i). In
347 contrast, P_{area} only had a significant positive influence on Vc_{max} (Table 3, Fig. S3f). Overall,
348 species identity significantly modulated the slope (for g_m and Vc_{max}) and the directionality of
349 the relationships towards N_{area} (for g_{sc}) (Table 3, Figs. S3a-c).

350 Based on a theoretical model, we analysed the direct and indirect influences of leaf
351 biometric and chemistry on photosynthetic processes and capacity. Our initial model assumed
352 that A_{sat} was directly constrained by g_{sc}, g_m and Vc_{max} but indirectly by LMA, N_{area} and P_{area}
353 (see Fig. 1). We assumed that g_{sc}, g_m and Vc_{max} covaried and were dependent on LMA, N_{area}
354 and P_{area}. Finally, N_{area} and P_{area} were a function of LMA. This initial model was not rejected
355 by observations for any species ($P_{model} = 0.22$). The model was improved ($P_{model} = 0.41$) when
356 we considered a direct path from LMA to A_{sat}, no relationship between P_{area}-Vc_{max} and P_{area}-g_m
357 and a causal relationship between $P_{area} \rightarrow g_{sc}$ (Figs. 6a,b,c).

358 When this model was applied to each species, we showed that the importance of paths
359 to explain A_{sat} variation differed between the three Salix species (Figs. 6a,b,c). Vc_{max} was the
360 most important causal variable among the direct controls to A_{sat} for *S. arctica* and *S. reticulata*
361 ($\rho_{vcmax} = 0.46$ vs $\rho_{vcmax} = 0.55$, respectively), except for *S. richardsonii* where g_{sc} played a
362 dominant role ($\rho_{gsc} = 0.42$ vs $\rho_{gm} = 0.37$ and $\rho_{vcmax} = 0.31$). Mesophyll conductance played a
363 direct and substantial role for explaining variation in A_{sat} for the three species (ρ_{gm}(*S. arc.*) =
364 0.33, ρ_{gm}(*S. ret.*) = 0.26, ρ_{gm}(*S. ric.*) = 0.37). Coordination among photosynthetic processes was
365 a key condition to model stability. N_{area} increased both Vc_{max} and g_m more substantially for *S.*
366 *reticulata* and *S. arctica* compared to *S. richardsonii*. LMA influenced positively g_{sc}, but had
367 a substantial negative influence on g_m. Finally, there was a weak positive influence of P_{area} on
368 g_{sc} for *S. richardsonii*, whereas a negative influence was observed for the two other species.

369 Path analyses showed contrasting photosynthetic regulatory pathways among species
370 which aligned with species differences in PNUE and iWUE models (r^2_m(PNUE) = 0.24,

r^2_c(PNUE) = 0.52; r^2_m(iWUE) = 0.24, r^2_c(iWUE) = 0.48, Figs. 6d,e). The highest PNUE was observed for *S. reticulata* (*S. reticulata* = 3.26 ± 0.09 µmol CO_2 g^{-1} N, *S. arctica* = 2.87 ± 0.14, *S. richardsonii* 2.43 ± 0.14 µmol CO_2 g^{-1} N, *P*-values of post-hoc differences among species were all < 0.05), and the highest iWUE for *S. richardsonii* (*S. richardsonii* = 74.7 ± 3.48, *S. arctica* = 65.5 ± 3.20, *S. reticulata* = 56.4 ± 3.19 µmol CO_2 $mmol^{-1}$ H_2O, *P*-values < 0.05).

Discussion

Arctic shrubs are important components of vegetation changes that currently occur across the Arctic tundra biome. This study aimed at exploring the variation of photosynthetic biochemical and diffusive capacities within and among three Salix species co-occurring in the High Arctic. We notably assessed the extent to which variation in leaf biometric and chemistry as well as in the diffusional and biochemical components of photosynthesis constrained A_{sat}. Our observational approach showed that A_{sat} measured under standard leaf micro-environmental conditions and at a standard site and date can strongly vary among individuals (1-18 µmol m^{-2} s^{-1}) and ~25% of this variation is attributable to N_{area}, species identity and their interaction within a low nitrogen availability Arctic tundra (Deschamps et al., 2022). When g_{sc}, g_m and Vc_{max} are coordinated, A_{sat} could reach higher values, comparable to other biomes.

Rare measurements of A_{sat} on Arctic shrubs

In the Arctic tundra of North-East Canada, we showed that the photosynthetic capacity of three shrub species, *S. arctica*, *S. reticulata* and *S. richardsonii* at leaf temperature of 10°C was on average 9.9 ±0.5, 11.1 ±0.4 and 8.7 ±0.5 µmol m^{-2} s^{-1}, respectively. Such light-saturated photosynthesis rates are also in the range of those reported for deciduous shrub species occurring at similar latitude and measured at saturating light conditions, ambient CO_2 concentration, and a leaf temperature of ~10°C. In the later studies, A_{sat} varied between 5.9 and 18.0 µmol m^{-2} s^{-1} and averaged 11.4±0.9 µmol m^{-2} s^{-1} for the following species and sites: *S. pulchra* in Barrow-Alaska (N71°, Rogers et al., 2017), *S. pulchra* and *S. reticulata* in Philip Smith Mountains –Alaska (N68°, Oberbauer et al., 1989), *S. arctica* in northwest Greenland (N76°, Leffler & Walker, 2013) and in northeast Greenland (N74°, Albert et al., 2011), *S. glauca* and *Betula glandulosa* in south Greenland (N61°, Simin et al., 2022), *S. glauca* and *Betula nana* in northern Sweden (N68°, Fletcher et al., 2012), *S. polaris* in Svalbard Island (N79°, Muraoka et al., 2002), *S. richardsonii*, *S. glauca* and *S. kolymensis* in Yakutia (N70°, Fan et al., 2018). This range of A_{sat} measured on Arctic species is above the values estimated by terrestrial biophysical models (A_{sat} = 6.75 ± 2.90 µmol m^{-2} s^{-1} corrected at 10°C from Rogers et al., 2017),

which used temperature functions with parameters approximated from dataset in which Arctic shrub species were underrepresented (Rogers et al., 2017). The same observation goes for the estimation of the carboxylation capacity, which averages at Vc_{max} = 28.2 ± 0.6 µmol m^{-2} s^{-1} in our study compared to 12.5 ± 5.6 µmol m^{-2} s^{-1} estimated at 10°C by terrestrial biophysical models in Rogers et al. (2017), as well as calculated by Kattge et al. (2009) from N_{area}-Vc_{max} equation for deciduous shrubs. Overall, these results emphasize the need to better constrain such key parameters in terrestrial models if we are to improve estimations of growth primary productivity in the Arctic tundra (Euskirchen et al., 2022).

Salix species are aligned along the leaf economic spectrum for most traits

In agreement with the leaf economic spectrum and earlier observations, Arctic Salix species showed higher LMA and lower PNUE in comparison with the worldwide database, hence highlighting the conservative strategy that Arctic plants use to cope with the cold environment of the tundra (Reich et al., 1992; Wright et al., 2004; Thomas et al., 2020). Among Salix individuals, leaf tissue investment trades off with leaf light-saturated photosynthetic capacity for a given nitrogen unit (Wright et al., 2002). Individuals with a conservative strategy (high LMA, low PNUE) have lower mesophyll conductance (Fig. S3h; Parkhurst, 1994; Xie et al., 2019) and lower N partition to photosynthetic components (Fig. S5; Poorter & Evans, 1998; Hikosaka & Hirose, 2000; Onoda et al., 2017), both of which constrain leaf photosynthesis while ensuring a higher leaf lifespan (Wright et al., 2004).

In contrast to what is expected based on the leaf economic spectrum and the Temperature-Biogeochemical hypothesis (Reich & Oleskyn, 2004), as well as the nutrient limitation usually observed in Arctic tundra (Elser et al., 2007; Deschamps et al., 2022 for Bylot island), the values of A_{sat}, N_{area} and P_{area} measured in this study were particularly high, which was highlighted when we compared Salix traits with those from the Globamax dataset (Fig. 2). As proposed by Reich & Oleskyn (2004), species inhabiting cold environments may exhibit high leaf nutrient concentrations as an adaptation to sustain carboxylation capacity. This is necessary because the biochemical efficiency of nitrogen-rich enzymes and phosphorus-rich RNA diminishes at low temperatures, as discussed by Woods et al. (2003). Rogers et al. (2017) argued that the high N_{area} of tundra species should allow A_{sat} to be two-fold higher than estimated by current Earth system models. Our findings support this assertion and suggest that the models need to be updated with region-specific data to more accurately reflect the photosynthetic capacity of tundra shrub species. In line with these considerations, our study showed that, independently of LMA values, the main contributor to A_{sat} variation was the

436 investment in nitrogen. In addition, we observed higher photosynthetic N use efficiency
437 (PNUE) with increasing P_{area}, which spatially extend the previously observed role of P to the
438 tundra biome (Maire et al., 2015; Ellsworth et al., 2023). However, this effect was less marked
439 than with increasing N_{area}, likely because P limitation could be considered weak in this recently
440 weathered valley of artic tundra (6000 cal yr BP, Fortier & Allard, 2004). As such, we suggest
441 that the economics of leaf nutrients (N_{area}-P_{area}-A_{sat}) should be studied concomitantly with the
442 economics of leaf organic matter (LMA-leaf dry matter content-leaf lifespan) in tundra.
443 Whereas both economic spectra are tightly coupled at large scale (Reich et al., 2014), having
444 long lifespan at low nutrient concentration for deciduous species may not be a successful
445 strategy when the vegetative period is highly constrained as in High Arctic tundra.

446 ***Carboxylation capacity is the main limitation of A_{sat} in Arctic Salix shrubs***

447 The three analytical approaches we used (c.f. sensitivity analysis, mixed interactive regression
448 model, path analysis) converged toward the same conclusion that carboxylation capacity was
449 the dominant limiting process to A_{sat} for the three Salix species in High Arctic tundra. Such
450 level of leaf biochemical limitation usually occurred in plant species with high A_{sat}, w hereas
451 both g_{sc} and g_m are considered major photosynthetic limitations in relatively low A_{sat} species
452 (Gago et al., 2023). This biochemical limitation may occur as low temperatures strongly limit
453 the enzymatic efficiency of RuBP carboxylation and because the nitrogen investment in
454 Rubisco proteins by the three Salix species was relatively low (11.9 ± 0.3%, calculated with
455 Eq. 4 from Niinemets & Tenhunen (1997) and normalized to 25°C) compared with global
456 variation (18.9 ± 6.2%, Onoda et al., 2017). While N could be invested to increase Vc_{max} (see
457 Fig. 6), it may also be required in proteins that protect against the continuous daylight stress of
458 the tundra environment (Mittler et al., 2022; Huang et al., 2004).

459 This primary limitation by biochemical processes occurred as stomatal and mesophyll
460 conductances of Salix species constrained only weakly the variation of A_{sat} at low temperature
461 (g_{sc} = 112.6 ± 4.5 mmol m^{-2} s^{-1}; g_m = 116.4 ± 4.2 mmol m^{-2} s^{-1}) when compared with another
462 study at a similar reference temperature of 10°C in Antarctica (g_{sc} = 78 ± 18 mmol m^{-2} s^{-1}, g_m
463 = 50 ± 14 mmol m^{-2} s^{-1}, Saez et al 2017) or with the meta-analysis by Knauer et al. (2022) for
464 deciduous angiosperms when expressed at 10°C using the temperature response of Bernacchi
465 et al. (2002) (g_m = 62.3 ± 8.3 mmol m^{-2} s^{-1}). While g_m was not the most limiting process
466 underlying the A_{sat} variation, we found that g_m was primarily positively and directly related to
467 leaf chemistry and N concentration, when controlling for LMA in the regression model. N
468 could increase the chloroplast surface area per unit leaf area, which increase CO_2 transport

469 through the cell (Onoda & Wright, 2018; Gao et al., 2022). Conversely, LMA significantly
470 decreased g_m as observed globally in Onoda & Wright (2018), but this appeared only after
471 considering N_{area} in the regression model. The negative effect of LMA on g_m was partly
472 explained by increases in leaf thickness and leaf dry matter content (see Table S2 and Figs.
473 S5). As such, our observations followed the expected trend in the literature (Niinemets et al.,
474 2009), but further leaf anatomical characterisation in Arctic Salix would be required to fully
475 understand the influence of LMA and particularly N_{area} on g_m.

476 The coordination between the photosynthetic reaction-diffusion processes, g_{sc}, g_m and
477 Vc_{max} was central to the successful execution of the path analysis routine as the model was
478 statistically rejected without considering it. We also observed a tight covariation between the
479 biochemical capacity for RuBP regeneration, J_{max}, and Vc_{max} (Fig. S2a, Table S1), which was
480 in line with previous studies (e.g. Walker et al., 2014). The coordination of photosynthetic
481 processes is usually observed and expected to be optimized through natural selection (e.g.
482 Maire et al., 2012; Flexas et al., 2015). Yet, after controlling this coordination, each of the
483 photosynthetic process has played an independent and substantial effect on A_{sat} and interacted
484 together to optimize A_{sat}. As such, the increase of A_{sat} with Vc_{max} and A_{sat} with g_m, i.e. the
485 increase in leaf C return for a given investment in nitrogen (considering that Vc_{max} and g_m
486 increased with N_{area}), was more rapid whenever stomata are fully open and more prone to lose
487 water. This resulted in a trade-off between the photosynthetic nitrogen use efficiency and the
488 intrinsic water use efficiency (see Fig. S5), which has been observed elsewhere in temperate
489 and dry ecosystems (Field et al., 1983; Hikosaka et al., 1998; Flexas & Carriqui, 2020), but
490 never in Arctic tundra to our knowledge.
491

492 ***Nitrogen-regulated species and stomatal-regulated species***

493 Unlike the limitation analysis, the path analyses distinguished two regulatory pathways for A_{sat}
494 among the co-occurring Salix species. To our knowledge, this is the first study to show these
495 two strategies of photosynthesis for Arctic species, optimizing either nitrogen or water
496 resource. Prostrate *S. arctica* and *S. reticulata,* whose dominance typically peaks in mesic
497 Arctic environments (Duclos, 2002), exhibited an N-regulatory pathway. New N units will
498 increase the photosynthetic capacity through both Vc_{max} and g_m processes, resulting in high
499 PNUE for both species (Figs. 6d, e). In contrast, erect *S. richardsonii*, which is adapted to moist
500 to wet habitats and predominates on alluvial fans in the valley (Duclos, 2002), showed A_{sat}
501 regulation mainly through stomatal conductance, resulting in higher iWUE compared to the
502 other two Salix species. Shrubification concerns both nitrogen-regulated and stomatal-

regulated species. *S. arctica* will be the first to colonize glacier retreat areas (Boulanger-Lapointe et al. 2014), while *S. richardsonii* will increase in height benefiting from climate warming (Buchkowski et al. 2020). Using leaf nitrogen to predict photosynthetic capacity in High Arctic tundra, terrestrial biosphere models have the correct formalism once calibrated for nitrogen-regulated species to simulate growth primary productivity (Rogers et al. 2017). However, neither the formalism nor the calibration appears to be appropriate for stomatal-regulated species, a problem that should be investigated in future research.

Conclusion

A core result of our study is that key shrub species in the High-Arctic tundra of Bylot island are characterized by higher light-saturated photosynthetic capacity than expected from global databases. Leaf N concentration emerged as the best leaf economic predictors of A_{sat} variation regulating both carboxylation capacity and mesophyll conductance. Such variation of N_{area} and A_{sat} needs to be better quantified across species and environmental conditions of the Arctic as it can have strong implication for the modelling of Arctic tundra vegetation in Earth system models.

Acknowledgements

The authors are thankful to the Inuit community of Pond Inlet and to Parks Canada-Sirmilik National Park, and grateful to D. Bouchard, E. Hardy-Lachance, F. Tanguay, V. Roy-Blais and C. Gignac, for their help with leaves harvests and measurements. This study was supported by the Fonds de recherche du Québec-Nature et technologies (FRQNT-2018-PR-208107), the Natural Sciences and Engineering Research Council of Canada (RGPIN-2023-05596), the Network of Centers of Excellence of Canada ArcticNet and the Northern Scientific Training Program (Indian and Northern Affairs Canada). Logistical support for fieldwork was provided by the Centre d'Études Nordiques (CEN) and Polar Continental Shelf Program (Natural Resources Canada).

Authors' contributions

J.P., V.M., S.P. and G.E. conceived and designed the research. J.P. collected the material and processed the measurements. J.P. and V.M. led the writing of the manuscript, with contributions of all co-authors.

References

Andresen CG, Lawrence DM, Wilson CJ, McGuire AD, Koven C, Schaefer K, Jafarov E, Peng S, Chen X, Gouttevin I, Burke E, Chadburn S, Ji D, Chen G, Hayes D, Zhang W. 2020. Soil moisture and hydrology projections of the permafrost region: a model intercomparison. *The Cryosphere* **14**: 445-459.

Baddeley JA, Woodin SJ, Alexander IJ. 1994. Effects of increased nitrogen and phosphorus availability on the photosynthesis and nutrient relations of three Arctic dwarf shrubs from Svalbard. *Ecology* **8**: 676-85.

Bernacchi CJ, Singsaas EL, Pimentel C, Portis AR, Long SP. 2001. Improved temperature response functions for models of rubisco-limited photosynthesis. *Plant, Cell and Environment* **24**: 253-59.

Bjorkman AD, Myers-Smith IH, Elmendrof SC, Normand S, Rüger N, Beck PSA, Blach-Overgaard A, Blok D, Cornelissen JHC, Forbes BC, et al. 2018. Plant functional trait change across a warming tundra biome. *Nature* **562**:57-62.

Bliss LC, Wein RW. 1972. Plant community responses to disturbances in the Western Canadian Arctic. *Canadian Journal of Botany* **50**:1097-109.

Box JE, Colgan WT, Christensen TR, Schmidt NM, Lund M, Parmentier FJW, Brown R, et al. 2019. Key indicators of Arctic climate change: 1971-2017. *Environmental Research Letters* **14**: 045-010.

Bredahl L, Ro-Poulsen H, Mikkelsen TN. 2004. Reduction of the ambient UV-B radiation in the High-Arctic increases Fv/Fm in *Salix arctica* and *Vaccinium uliginosum* and reduces stomatal conductance and internal CO_2 concentration in *Salix arctica*. *Arctic, Antarctic, and Alpine Research* **36**:364-369.

Boulanger-Lapointe N, Lévesque E, Boudreau S, Henry GHR, Schmidt NM. 2014. Population structure and dynamics of Arctic willow (*Salix arctica*) in the High-Arctic. *Journal of Biogeography* **41**(10):1967-1978.

Buchkowski RW, Morris DW, Halliday WD, Dupuch A, Morrissette-Boileau C, Boudreau S. 2020. Warmer temperatures promote shrub radial growth but not cover in the central Canadian Arctic. *Arctic, Antarctic, and Alpine Research* **52**(1): 582-595.

Chapin FSIII, Shaver GR, Giblin AE, Nadelhoffer KJ, Laundre JA. 1995. Responses of Arctic tundra to experimental and observed changes in climate. *Ecology* **76**: 694-711.

Chapin FSIII, Shaver GR. 1989. Differences in growth and nutrient use among Arctic plant growth forms. *Functional Ecology* **3**: 73-80.

Chapin FSIII, Shaver GR. 1996. Physiological and growth responses of Arctic plants to a field experiment simulating climatic change. *Ecology* **77**: 822-840.

Coulombe S, Fortier D, Bouchard F, Paquette M, Charbonneau S, Lacelle D, Laurion I, Pienitz R. 2022. Contrasted geomorphological and limnological properties of thermokarst lakes formed in buried glacier ice and ice-wedge polygon terrain. *Cryosphere* **16**: 2837-57.

Deschamps L, Maire V, Chen L, Fortier D, Gauthier G, Morneault A, Hardy-Lachance E, Dalcher-Gosselin I, Tanguay F, Gignac C, McKenzie JM, Rochefort L, Lévesque E. 2022. Increased nutrient availability speeds up permafrost development, while goose

grazing slows it down in a Canadian High Arctic wetland. *Journal of Ecology* **111**:449-463.

Díaz S, Kattge J, Cornelissen JHC, Wright IJ, Lavorel S, Dray S, Reu B, *et al.* 2016. The global spectrum of plant form and function. *Nature* **529**: 167-71.

Domine F, Lackner G, Sarrazin D, Poirier M, and Belke-Brea M. 2021. Meteorological, snow and soil data (2013-2019) from a herb tundra permafrost site at Bylot island, canadian High Arctic, for driving and testing snow and land surface models. *Earth System Science Data* **13**: 4331-48.

Duclos I. 2002. Milieux mésiques et secs de l'île bylot, nunavut (canada) : caractérisation et utilisation par la grande oie des neiges. MSc thesis, Université du Québec à Trois-Rivières, Trois-Rivières, QC, Canada.

Elferjani R, Benomar L, Momayyezi M, Tognetti R, Niinemets Ü, Soolanayakanahally RY, Théroux-Rancourt G, *et al.* 2021. A meta-analysis of mesophyll conductance to CO_2 in relation to major abiotic stresses in poplar species. *Journal of Experimental Botany* **72**: 4384–4400.

Ellis CJ, and Rochefort L. 2004. Century-scale development of polygon-patterned tundra wetland, Bylot Island (73°N, 80°W). *Ecology* **85** (4): 963-78.

Ellsworth DS, Crous KY, de Kauwe MG, Verryckt LT, Goll D, Zaehle S, Bloomfield KJ, Ciais P, Cernusak LA, Domingues TF, Dusenge ME, Garcia S, Guerrieri R, Ishida FY, Janssens IA, Kenzo T, Ichie T, Medlyn BE, Meir P, Wright IJ. 2022. Convergence in phosphorus constraints to photosynthesis in forests around the world. *Nature Communications* **13**: 5005.

Euskirchen ES, Serbin SP, Carman TB, Fraterrigo JM, Genet H, Iversen CM, Salmon V, McGuire AD. 2022. Assessing dynamic vegetation model parameter uncertainty across Alaskan Arctic tundra plant communities. *Ecological Applications* **32**(2): e2499.

Evans JR, von Caemmerer S. 2013. Temperature response of carbon isotope discrimination and mesophyll conductance in tobacco. *Plant, Cell and Environment* **36**: 745-756.

Fan R, Morozumi T, Maximov TC, Sugimoto A. 2018. Effect of floods on the δ13C values in plant leaves: a study of willows in Northeastern Siberia. *PeerJ* **6**: e5374.

Fatichi S, Leuzinger S, Körner C. 2014. Moving beyond photosynthesis: from carbon source to sink-driven vegetation modeling. *New Phytologist* **201**: 1086-95.

Fernández-Marín B, Gulías J, Figueroa CM, Iñiguez C, Clemente-Moreno MJ, Nunes-Nesi A, Fernie AR, *et al.* 2020. How do vascular plants perform photosynthesis in extreme environments? an integrative ecophysiological and biochemical story. *Plant Journal* **101**: 979-1000.

Firn J, McGree JM, Harvey E, Flores-Moreno H, Schütz M, Buckley YM, Borer ET, *et al.* 2019. Leaf nutrients, not specific leaf area, are consistent indicators of elevated nutrient inputs. *Nature Ecology and Evolution*. doi: 10.1038/s41559-018-0790-1.

Fletcher BJ, Gornall JL, Poyatos R, Press MC, Stoy PC, Huntley B, Baxter R, and Phoenix GK. 2012. Photosynthesis and productivity in heterogeneous Arctic tundra: consequences for ecosystem function of mixing vegetation types at stand edges. *Journal of Ecology* **100**: 441-51.

Gago J, Daloso DM, Figueroa CM, Flexas J, Fernie AR, & Nikoloski Z. 2016. Relationships of leaf net photosynthesis, stomatal conductance, and mesophyll

conductance to primary metabolism: A multispecies meta-analysis approach. *Plant Physiology*, **171**: 265-279.

Gago J, Daloso DM, Carriquí M, Nadal M, Morales M, Araújo WL, Nunes-Nesi A, Perera-Castro AV, Clemente-Moreno MJ & Flexas J. 2020. The photosynthesis game is in the "inter-play": Mechanisms underlying CO_2 diffusion in leaves. *Environmental and Experimental Botany*. doi: 10.1016/j.envexpbot.2020.104174

Gago J, Nadal M, Clemente-Moreno MJ, Figueroa CM, Medeiros DB, Cubo-Ribas N, Cavieres LA, Gulías J, Fernie AR, Flexas J, Bravo LA. 2023. Nutrient availability regulates *Deschampsia antarctica* photosynthetic and stress tolerance performance in Antarctica. Journal of Experimental Botany, **74**: 2620-2637.

Galmés J, Capó-Bauçà S, Niinemets Ü, Iñiguez C. 2019. Potential improvement of photosynthetic CO_2 assimilation in crops by exploiting the natural variation in the temperature response of rubisco catalytic traits. *Current Opinion in Plant Biology* **49**: 60-67.

Galmés J, Hermida-Carrera C, Laanisto L, Niinemets Ü. 2016. A compendium of temperature responses of rubisco kinetic traits: variability among and within photosynthetic groups and impacts on photosynthesis modeling. *Journal of Experimental Botany* **67**: 5067-91.

Galmés J, 0Medrano H, Flexas J. 2007. Photosynthetic limitations in response to water stress and recovery in Mediterranean plants with different growth forms. *New Phytologist* **175**: 81-93.

Gauthier G, Hughes RJ, Reed A, Beaulieu J. 1995. Effect of grazing by greater snow geese on the production of graminoids at an Arctic site (Bylot Island, NWT, Canada). *Journal of Ecology* **83**: 653-664.

Gignac C, Rochefort L, Gauthier G, Lévesque E, Maire V, Deschamps L, Pouliot R, Marchand-Roy M. 2022. N/P Addition Is More Likely Than N Addition Alone to Promote a Transition from Moss-Dominated to Graminoid-Dominated Tundra in the High-Arctic. Atmosphere. *Atmosphere* **13**:676. https://doi.org/10.3390/atmos13050676

Givnish TJ. 1986. Optimal stomatal conductance, allocation of energy between leaves and roots, and the marginal cost of transpiration. In: Givnish TJ, eds. *On the Economy of Plant Form and Function*. Cambridge, UK: Cambridge Univ Press 171-213.

Godin E, Fortier D. 2012. Geomorphology of a thermo-erosion gully, Bylot Island, Nunavut, Canada. *Canadian Journal of Earth Sciences* **49**: 979–86.

Grassi G, Magnani F. 2005. Stomatal, mesophyll conductance and biochemical limitations to photosynthesis as affected by drought and leaf ontogeny in ash and oak trees. *Plant, Cell and Environment*, **28**: 834-849.

Harwood R, Théroux-Rancourt G, Barbour MM. 2021. Understanding airspace in leaves: 3D anatomy and directional tortuosity. *Plant Cell and Environment*. 44(8): 2455-2465.

Hikosaka K, 2010. Mechanisms underlying interspecific variation in photosynthetic capacity across wild plant species. *Plant Biotechnology*, **27**: 223-229.

Hughes RJ, Reed A, Gauthier G. 1994. Space and habitat use by greater snow goose broods on Bylot Island, Northwest Territories. *The Journal of Wildlife Management*. **58**: 536-545

Johnson DA, Tieszen LL. 1976. Aboveground biomass allocation, leaf growth, and photosynthesis patterns in tundra plant forms in Arctic Alaska. *Oecologia* **24**: 159-173.

Kattge J, Knorr W. 2007. Temperature acclimation in a biochemical model of photosynthesis: A reanalysis of data from 36 Species. *Plant, Cell and Environment* **30**: 1176-90.

Kattge J, Knorr W, Raddatz T, Wirth C. 2009. Quantifying photosynthetic capacity and its relationship to leaf nitrogen content for global-scale terrestrial biosphere models. *Global Change Biology* **15**: 976-991.

Kirschbaum MUF, Farquhar GD. 1987. Investigation of the CO_2 dependence of quantum yield and respiration in eucalyptus pauciflora. *Plant Physiology* **83**:1032-1036.

Knauer J, Cuntz M, Evans JR, Niinemets Ü, Tosens T, Veromann-Jürgenson LL, Werner C, Zaehle S. 2022. Contrasting anatomical and biochemical controls on mesophyll conductance across plant functional types. *New Phytologist* **236**: 357-68.

Kong RS, Way DA, Henry HAL, Smith NG. 2022. Stomatal conductance, not biochemistry, drives low temperature acclimation of photosynthesis in *Populus balsamifera*, regardless of nitrogen availability. *Plant Biology* **4**: 766-79.

Körner C. 1999. *Alpine Plant Life. Alpine Plant Life*. Springer International Publishing.

Körner C. 2015. Paradigm Shift in Plant Growth Control. *Current Opinion in Plant Biology* **25**: 107-14.

Kumarathunge DP, Medlyn BE, Drake JE, Tjoelker MG, Aspinwall MJ, Battaglia M, Cano FJ, *et al.* 2019. Acclimation and adaptation components of the temperature dependence of plant photosynthesis at the global scale. *New Phytologist* **222**: 768-84.

Lamarque LJ, Félix-Faure J, Deschamps L, Lévesque E, Cusson PO, Fortier, D, Giacomazzo M, Guillemette F, Paillassa J, Tremblay M, & Maire V. 2023. Hydrological regime and plant functional traits jointly mediate the influence of salix spp. on soil organic carbon stocks in a high arctic tundra. *Ecosystems* **26**: 1–-22.

Luo Y, Peng Q, Li K, Gong Y, Liu Y, Han W. 2021. Patterns of nitrogen and phosphorus stoichiometry among leaf, stem and root of desert plants and responses to climate and soil factors in Xinjiang, china. *Catena* **199**: 105100.

Luo X, Keenan TF, Chen JM, Croft H, Colin Prentice I, Smith NG, Walker AP, Wang H, Wang R, Xu C, Zhang Y. 2021. Global variation in the fraction of leaf nitrogen allocated to photosynthesis. *Nature Communications* **12**:1. https://doi.org/10.1038/s41467-021-25163-9

Leffler AJ, Welker JM. 2013. Long-term increases in snowpack elevate leaf N and photosynthesis in Salix arctica: Responses to a snow fence experiment in the High Arctic of NW Greenland. *Environmental Research Letters*, **8**: 025023.

Maire V, Martre P, Kattge J, Gastal F, Esser G, Fontaine S, Soussana JF. 2012. The coordination of leaf photosynthesis links C and N fluxes in C3 plant species. *Plos One*, **7**: 15.

Maire V, Wright IJ, Prentice IC, Batjes NH, Bhaskar R, van Bodegom PM, Cornwell WK, Ellsworth D, Niinemets Ü, Ordonez A, Reich PB, Santiago LS. 2015. Global effects of soil and climate on leaf photosynthetic traits and rates. *Global Ecology and Biogeography* **24**: 706–-717.

Mbufong HN, Lund M, Aurela M, Christensen TR, Eugster W, Friborg T, Hansen BU, *et al.* 2014. Assessing the Spatial Variability in Peak Season CO_2 exchange Characteristics across the Arctic Tundra Using a Light Response Curve Parameterization. *Biogeosciences* **11**: 4897-4912.

Mooney HA, and Billings WD. 1961. Comparative Physiological Ecology of Arctic and Alpine Populations of *Oxyria Digyna. Ecological Monographs*, **31:** 1-29

Muraoka H, Uchida M, Mishio M, Nakatsubo T, Kanda H, Koizumi H. 2002. Leaf Photosynthetic Characteristics and Net Primary Production of the Polar Salix (*Salix Polaris*) in a High Arctic Polar Semi-Desert, Ny-Ålesund, Svalbard. *Canadian Journal of Botany* **80**: 1193-1202.

Myers-Smith IH, Hik DS. 2018. Climate Warming as a Driver of Tundra Shrubline Advance. *Journal of Ecology* **106**: 547-60.

Nishizawa, K, Deschamps L, Maire V, Bêty J, Lévesque E, Kitagawa R & Mori, A. S. 2021. Long-term consequences of goose exclusion on nutrient cycles and plant communities in the High-Arctic. *Polar Science* **27**:100631.

Oechel WC, Cowles S, Grulke N, Hastings SJ, Lawrence B, Prudhomme T, Riechers G, Strain B, Tissue D, Vourlitis G. 1994. Transient Nature of CO_2 Fertilization in Arctic Tundra. *Nature* **371:**500-503.

Onoda Y, Wright IJ, Evans JR, Hikosaka K, Kitajima K, Niinemets Ü, Poorter H, Tosens T, Westoby M. 2017. Physiological and Structural Trade-offs Underlying the Leaf Economics Spectrum. *New Phytologist* **214**: 1447-63.

Onoda Y, Wright IJ. 2018. The leaf economics spectrum and its underlying physiological and anatomical principles. *The leaf: a platform for performing photosynthesis* **44**: 451-471.

Paillassa J, Wright, IJ, Prentice IC, Pepin S, Smith NG, Ethier G, Westerband AC, Lamarque LJ, Han W, Cornwell WK, Maire V. 2020. When and where soil is important to modify the carbon and water economy of leaves. *New Phytologist* **228**: 121-135.

Pouliot R, Rochefort L, Gauthier G. 2009. Moss carpets constrain the fertilizing effects of herbivores on graminoid plants in Arctic polygon fens. *Botany* **87**: 1209–22.

Rantanen M, Karpechko AY, Lipponen A, Nordling K, Hyvärinen O, Ruosteenoja K, Vihma T, and Laaksonen A. 2022. The Arctic has warmed nearly four times faster than the globe since 1979. *Communications Earth & Environment* **3**: 168.

Reich PB, Oleksyn J. 2004. Global patterns of plant leaf N and P in relation to temperature and latitude. *Proceedings of the National Academy of Sciences*, **101**:11001-11006.

Reich PB, Oleksyn J, Wright IJ. 2009. Leaf phosphorus influences the photosynthesis-nitrogen relation: a cross-biome analysis of 314 species. *Oecologia* **160**: 207-12.

Reich PB. 2014. The world-wide "fast-slow" plant economics spectrum: A traits manifesto. *Journal of Ecology*, **102**: 275-301.

Reich PB, Sendall KM, Stefanski A, Rich RL, Hobbie SE, Montgomery RA. 2018. Effects of climate warming on photosynthesis in boreal tree species depend on soil moisture. *Nature*. **562**: 263-267.

Rogers A, Serbin SP, Ely KS, Sloan VL, Wullschleger SD. 2017. Terrestrial biosphere models underestimate photosynthetic capacity and CO_2 assimilation in the Arctic. *New Phytologist* **216**: 1090-1103.

Sáez PL, Bravo LA, Cavieres LA, Vallejos V, Sanhueza C, Font-Carrascosa M, Gil-Pelegrín E, Peguero-Pina JJ, Galmés J. 2017. Photosynthetic limitations in two antarctic vascular plants: importance of leaf anatomical traits and rubisco kinetic parameters. *Journal of Experimental Botany* **68**: 2871-83.

Sáez PL, Galmés J, Ramírez CF, Poblete L, Rivera BK, Cavieres LA, Clemente-Moreno MJ, Flexas J, Bravo LA. 2018. Mesophyll conductance to CO_2 is the most significant limitation to photosynthesis at different temperatures and water availabilities in antarctic vascular species. *Environmental and Experimental Botany* **156**: 279-87.

Segal AD, Sullivan PF. 2014. Identifying the sources and uncertainties of ecosystem respiration in Arctic tussock tundra. *Biogeochemistry* **121**: 489-503.

Théroux-Rancourt G, Gilbert ME. 2017. The light response of mesophyll conductance is controlled by structure across leaf profiles. *Plant Cell and Environment* **40**: 726-40.

Thomas HJD, Bjorkman AD, Myers-Smith IH, Elmendorf SC, Kattge J, Diaz S, Vellend M, *et al.* 2020. Global plant trait relationships extend to the climatic extremes of the tundra biome. *Nature Communications* **11**: 1351.

Walker AP, Beckerman AP, Gu L, Kattge J, Cernusak LA, Domingues TF, Scales JC, Wohlfahrt G, Wullschleger SD, Woodward FI. 2014. The relationship of leaf photosynthetic traits - Vcmax and Jmax - to leaf nitrogen, leaf phosphorus, and specific leaf area: a meta-analysis and modeling study. *Ecology and Evolution* **4**: 3218-35.

Walther S, Guanter L, Heim B, Jung M, Duveiller G, Wolanin A, Sachs T. 2018. Assessing the Dynamics of Vegetation Productivity in Circumpolar Regions with Different Satellite Indicators of Greenness and Photosynthesis. *Biogeosciences* **15**: 6221-56.

Woods HA, Makino W, Cotner JB, Hobbie SE, Harrison JF, Acharya K, & Elser JJ. 2003. Temperature and the chemical composition of poikilothermic organisms. Functional Ecology, **17**: 237-245.

Wright IJ, Reich PB, Westoby M, Ackerly DD, Baruch Z, Bongers F, Cavender-Bares J, *et al.* 2004. The worldwide leaf economics spectrum. *Nature* **428**:821-27.

Xie K, Lu Z, Pan Y, Gao L, Hu P, Wang M, Guo S. 2020. Leaf photosynthesis is mediated by the coordination of nitrogen and potassium: the importance of anatomical-determined mesophyll conductance to CO2 and carboxylation capacity. *Plant Science* **290**: 110267.

Zhang Y, Chen C, Jin Z, Yang Z, Li Y. 2022. Leaf anatomy, photosynthesis, and chloroplast ultrastructure of Heptacodium miconioides seedlings reveal adaptation to light environment. *Environmental and Experimental Botany*, **195**: 104780.

Zoltai SC. 1983. Pingos on Bylot Island, N. W. T., Canada *Polarforschung* **53**: 43-48.

Tables

Table 1: Statistics from a mixed regression model testing the influence of functional trait and nutrient economic traits on the leaf light-saturated photosynthetic capacity, A_{sat} and photosynthetic nitrogen use efficiency, PNUE (A_{sat}/N_{area}). We considered site and sampling date as random factors, and LMA, N_{area}, P_{area} and species as fixed factors. For fixed factors, we considered interactions between factor pairs and finally selected the model with the minimum of pairs that minimized the AIC criterion. We used the Gaussian family distribution for both A_{sat} and PNUE (n = 157). We did not consider N_{area} as an explicative variable in the PNUE model.

	A_{sat}			PNUE		
Model factors	**DF**	**F-value**	**P-value**	**DF**	**F-value**	**P-value**
Species	2	0.32	ns	2	5.91	**
N_{area}	1	25.81	***	—	—	—
P_{area}	1	8.17	**	1	10.38	**
LMA	1	11.42	***	1	38.63	***
N_{area} * Species	2	7.04	**	—	—	—
P_{area} * Species	2	2.13	ns	1	0.55	ns
Overall	$r^2_m = 0.26$; $r^2_c = 0.60$; AICC = 753			$r^2_m = 0.30$; $r^2_c = 0.30$; AICC = 395		

Table 2: Summary of the generalized mixed regression model testing the effect of biochemical vs. diffusive limitations (Vc_{max}, g_{sc}, g_m) on leaf light-saturated photosynthetic capacity, A_{sat}. We considered site and sampling date as random factors and used a gamma family distribution. We scaled the values of fixed factors to estimate their relative influence on A_{sat} variations. '***', $P < 0.001$; '**', $P < 0.01$; '*', $P < 0.05$; 'ns' $P > 0.1$.

Variable	***S. arctica***			***S. reticulata***			***S. richardsonii***			***All***		
	Est.	**SE**	**p.val.**	**Est.**	**SE**	**p.val.**	**Est.**	**SE**	**p.val.**	**Est.**	**SE**	**p.val.**
intercept	9.88	0.15	***	11.33	0.17	***	9.02	0.27	***	10.08	0.13	***
Vc_{max}	1.94	0.25	***	1.77	0.16	***	0.86	0.24	**	1.54	0.13	***
g_{sc}	1.13	0.17	***	0.51	0.13	***	1.16	0.24	***	1.05	0.11	***
g_m	1.31	0.21	***	0.94	0.18	***	1.38	0.25	***	1.28	0.12	***
$g_{sc}*g_m$	-0.38	0.24	ns	-0.09	0.14	ns	-0.63	0.32	*	-0.38	0.11	**
$g_{sc}*Vc_{max}$	0.73	0.29	*	-0.09	0.12	ns	0.41	0.23	*	0.31	0.12	***
g_m*Vc_{max}	-0.24	0.25	ns	0.02	0.11	ns	-0.11	0.28	ns	0.03	0.12	ns
$g_{sc}*g_m*Vc_{max}$	-0.05	0.13	ns	-0.15	0.12	ns	0.31	0.22	ns	0.06	0.07	ns
Overall	$r^2_m = 0.98$			$r^2_m = 0.96$			$r^2_m = 0.95$			$r^2_m = 0.98$		

Table 3: Statistics from a mixed regression model testing the influence of nutrient economic traits on the photosynthetic processes, g_s, g_m, Vc_{max}. We considered site and sampling date as random factors, and LMA, N_{area}, P_{area} and species as fixed factors. For fixed factors, we considered interactions between factor pairs and finally selected the model with the minimum of pair that minimized the AIC criterion. We used the Gaussian family distribution for all dependent variables and n = 157.

		g_s		g_m		Vc_{max}	
Model factors	**DF**	**F-value**	**P-value**	**F-value**	**P-value**	**F-value**	**P-value**
Species	2	4.15	*	0.75	ns	0.21	ns
N_{area}	1	1.82	ns	20.78	***	24.37	***
P_{area}	1	0.55	ns	2.46	ns	9.24	**
LMA	1	0.55	ns	10.83	**	13.24	***
N_{area} * Species	2	6.17	**	4.04	*	4.63	*
P_{area} * Species	2	3.12	°	2.07	°	0.23	ns
Overall		$r^2_m = 0.19$; $r^2_c = 0.61$ AICc = 1586		$r^2_m = 0.18$; $r^2_c = 0.50$ AICc = 1589		$r^2_m = 0.22$; $r^2_c = 0.53$ AICc = 988	

Figures

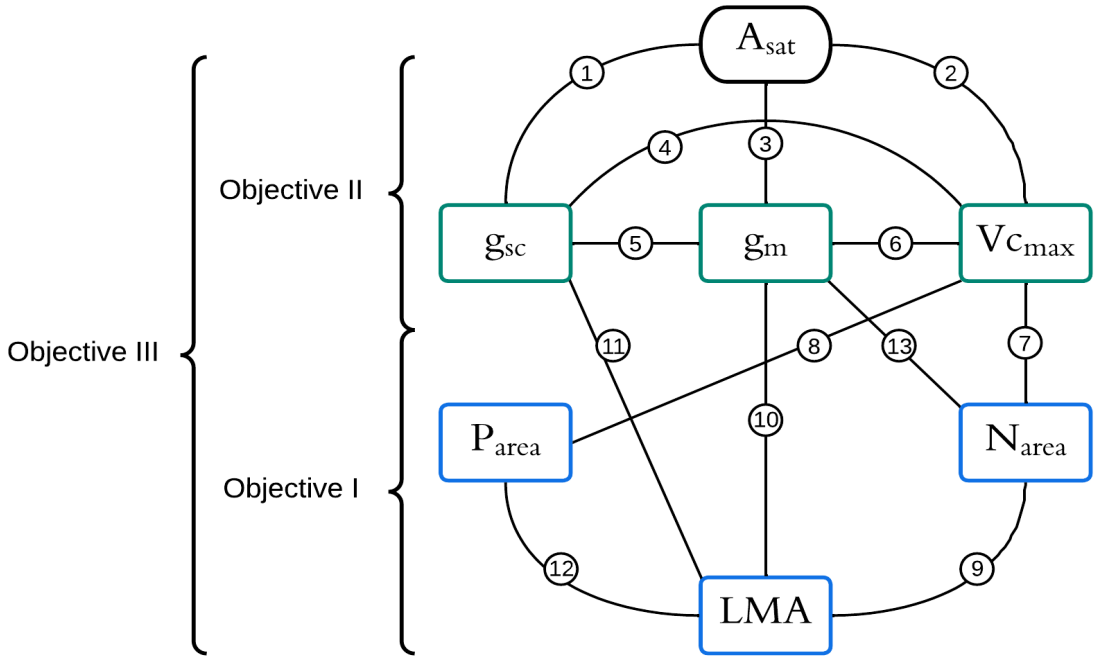

Figure 1: Conceptual model of relationships relating leaf photosynthetic capacity (A_{sat}) to leaf physiological processes (g_{sc}, g_m, Vc_{max}; green boxes) and morphological and chemical traits (N_{area}, P_{area}, LMA; blue boxes). Based on the literature, we considered the following paths: (1) stomatal conductance to CO_2, g_{sc}, constrains A_{sat} by regulating the entry of CO_2 substrate from the atmosphere into the leaf; (2) the maximum rate of CO_2 fixation by Rubisco in the Calvin cycle, Vc_{max}, determines A_{sat} by transforming CO_2 substrate into sucrose product; (3) mesophyll conductance, g_m, constrains A_{sat} by facilitating the diffusion of CO_2 through air and liquid cell medium to Rubisco; (4-6) coordination between g_{sc}, g_m and Vc_{max} processes is expected to optimize A_{sat} through natural selection (Givnish, 1986; Reich, 2014); (7) leaf nitrogen affects Vc_{max} through the requirement in nitrogen for photosynthetic enzymes (Field & Mooney 1986; Kattge et al 2009); (8) leaf phosphorus influences Vc_{max} through its requirement for the regeneration of the ribulose diphosphate, a key substrate for Rubisco as well as for Vc_{max} balance with the electron transport capacity (Ellsworth et al 2023); (9, 12) N_{area} and P_{area} are the mathematical products of LMA with N_{mass} and P_{mass}, respectively; (10) LMA impacts directly on mesophyll conductance through leaf anatomy (e.g. thickness of spongy and palisade tissue, Zhang et al. 2022 ; and mesophyll tortuosity, Harwood et al., 2021); (11) relationship between g_s and LMA which determines the thermal exchange of the leaf with the air and the soil and therefore the transpiration of the leaf (Gago et al., 2016); (13) leaf nitrogen affects g_m through the allocation of nitrogen to cellular and photosynthetic components (Onoda et al., 2015; Onoda & Wright, 2018; Gago et al., 2020).

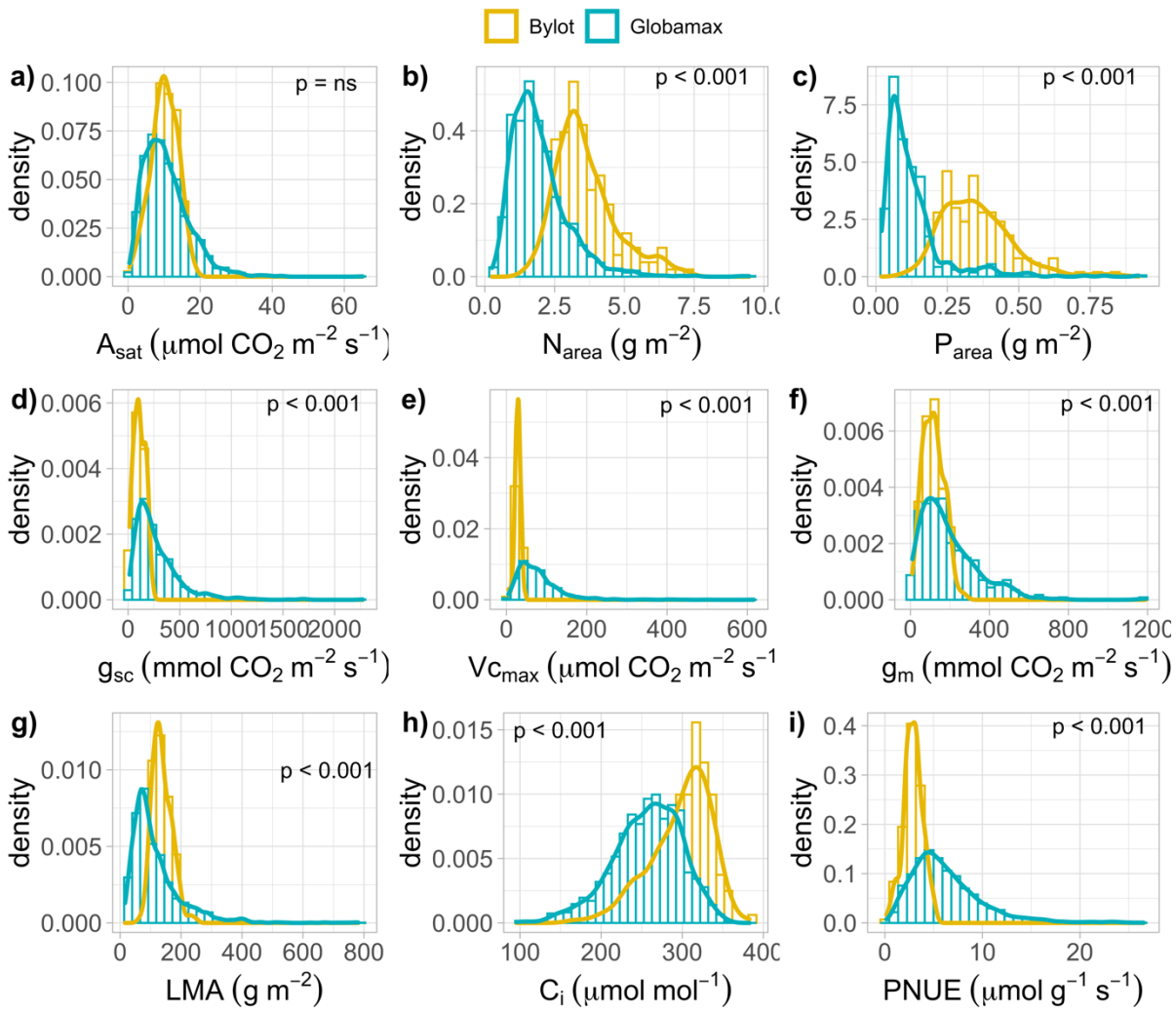

Figure 2: Variation of diffusional vs. biochemical limitations of photosynthesis and their underlying morphological and chemical determinants in Salix species from Bylot Island (73°09'N, 79°57'W) (n = 162) in comparison with corresponding photosynthetic traits from the Globamax database (n = 2409). Panels represent the variation of A_{sat}, g_{sc}, g_m, Vc_{max}, N_{area}, P_{area}, LMA, C_i and PNUE, respectively, for our study (yellow) and the Globamax database (blue).

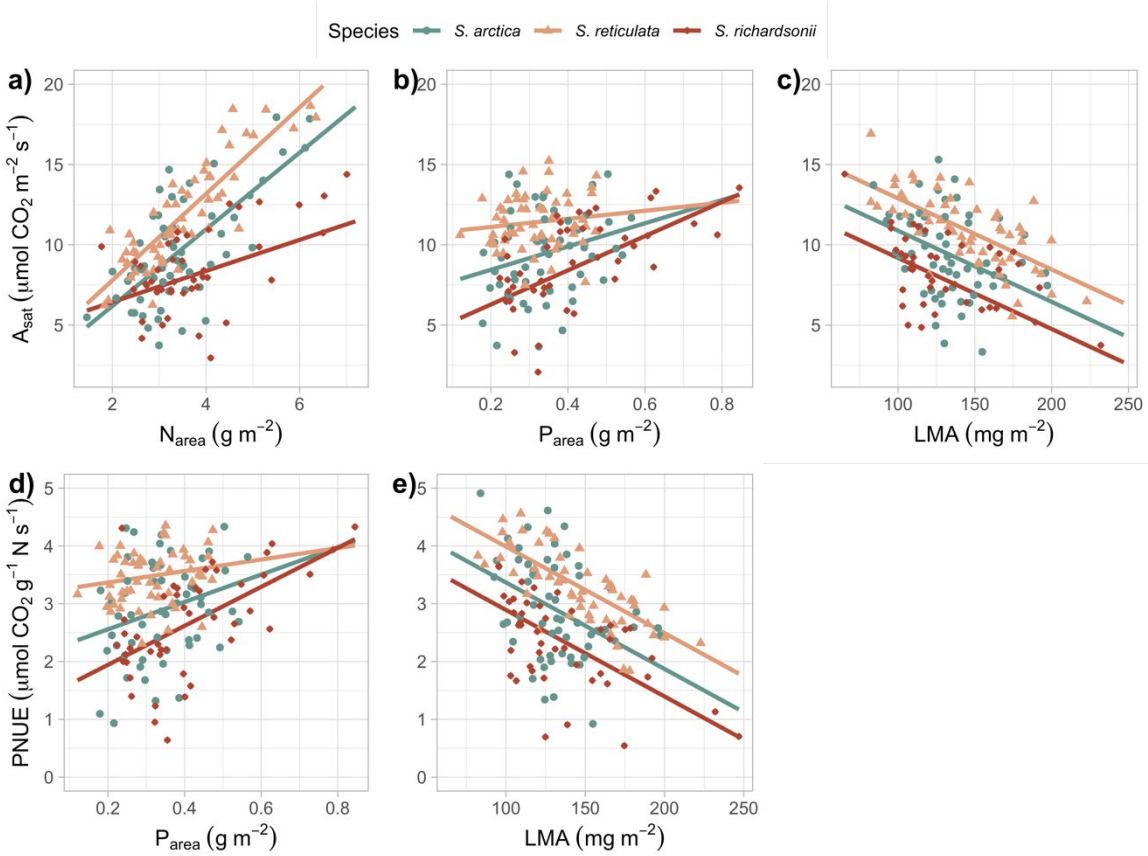

Figure 3: Conditional relationships from two mixed regression models testing the influence of morphological and nutrient economic traits on the leaf light-saturated photosynthetic capacity, A_{sat} and leaf photosynthetic nitrogen use efficiency, PNUE = A_{sat}/N_{area}. Relationships from the model explaining A_{sat} are presented in panels (a) leaf nitrogen concentration per unit area (N_{area}); (b) leaf phosphorus concentration per unit area (P_{area}); (c) leaf mass per unit area (LMA). Relationships from the model explaining PNUE are presented in panels (d) leaf phosphorus concentration per unit area (P_{area}) and (e) leaf mass per unit area (LMA). Relationships were from the generalized linear models presented in Table 1.

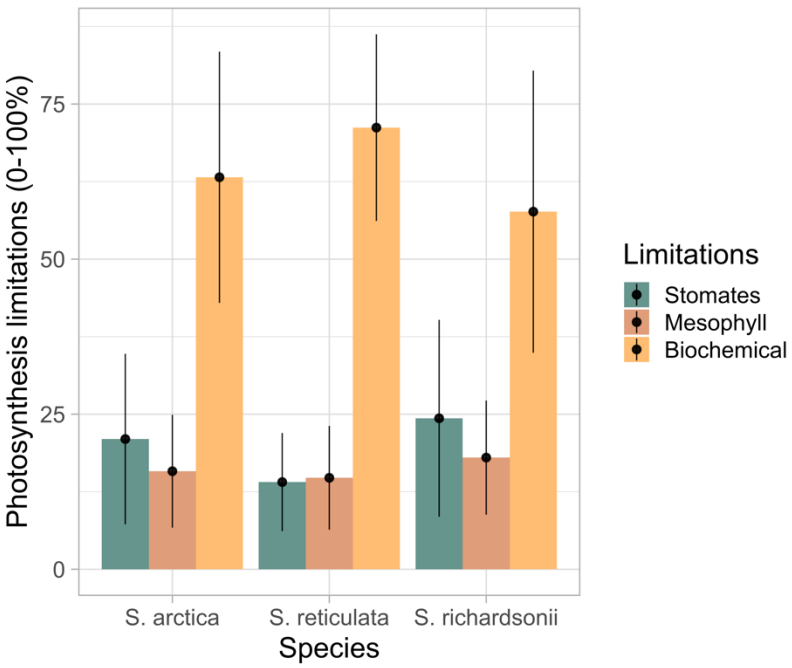

Figure 4: Biophysical and biochemical limitations of leaf photosynthesis in three Arctic *Salix* species : Stomatal (Ls), mesophyll (Lm), and biochemical (Lb) limitations (means ± SD) are shown.

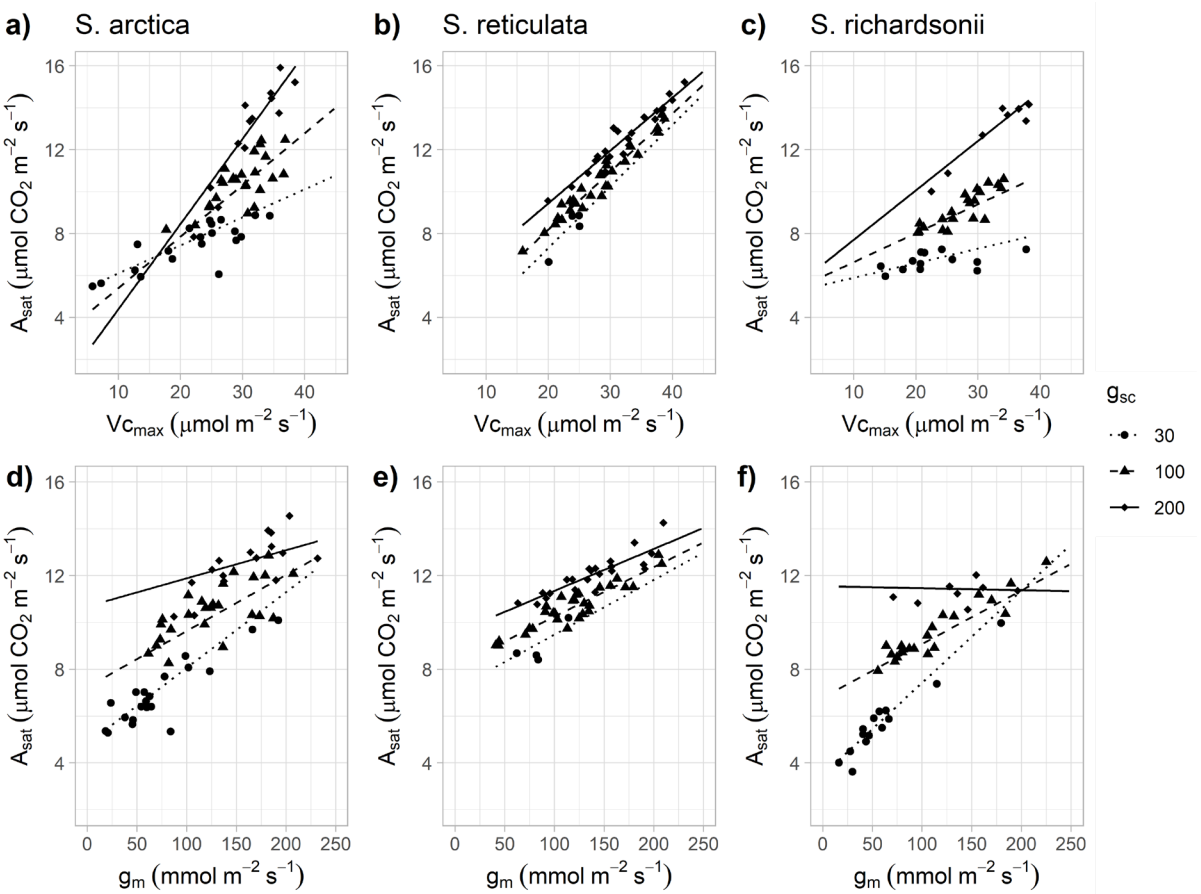

Figure 5: Conditional relationships between leaf light-saturated photosynthetic capacity (A_{sat}) and biophysical and biochemical photosynthetic processes for each Salix species. In panels a-c, relationships between Vc_{max} and A_{sat} are considered by species for three different values of g_{sc} (30, 100 and 200 mmol m^{-2} s^{-1}) with g_m set at its median value, 114 mmol m^{-2} s^{-1}. In panels d-f, relationships between g_m and A_{sat} are considered by species for different values of g_{sc} with Vc_{max} set at its median value, 28.7 µmol m^{-2} s^{-1}. Conditional relationships were fitted using generalized regression models of Table 3. Models considered sampling date and site as random factors and used a gamma distribution of A_{sat} values.

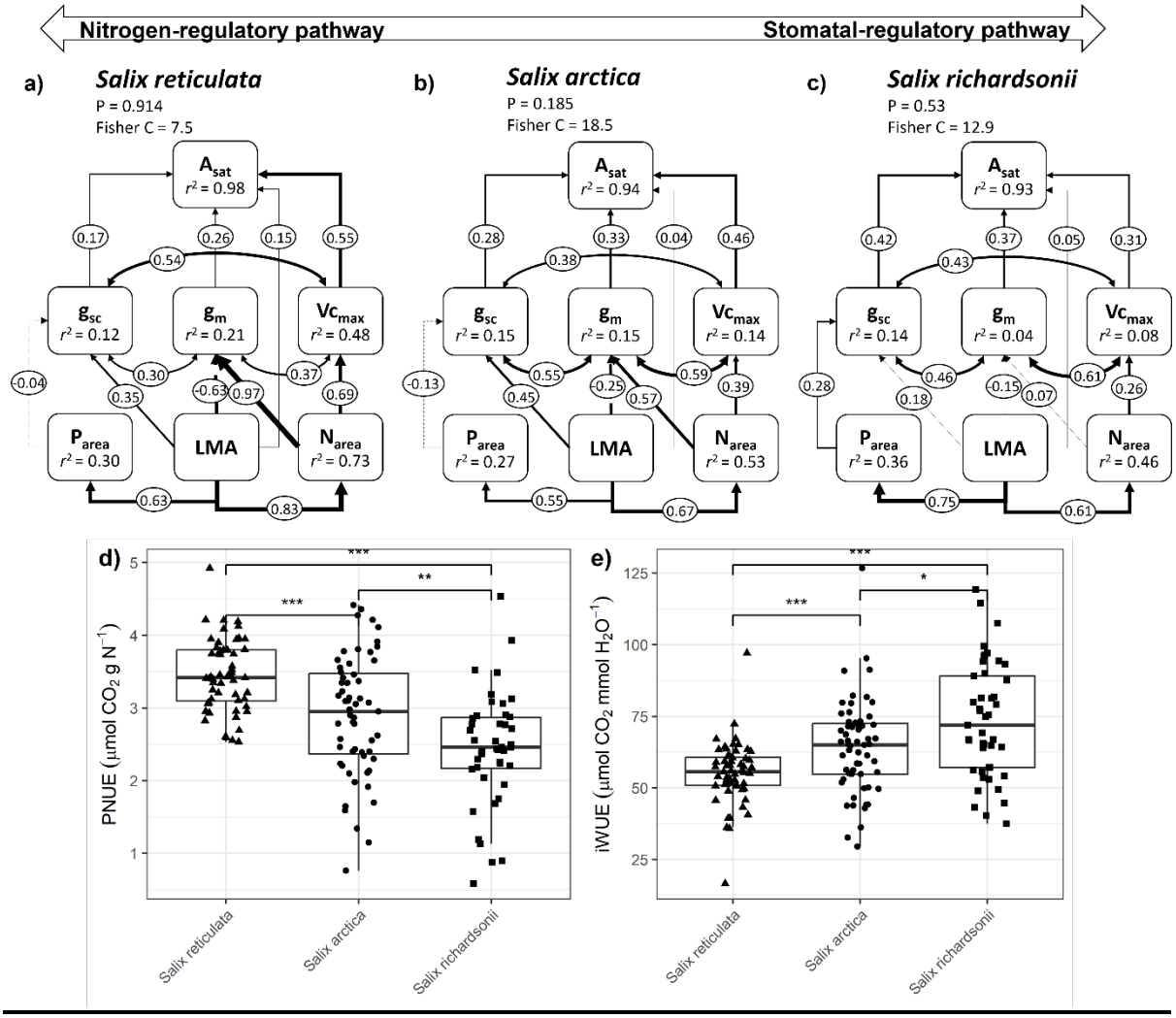

Figure 6: Regulation pathway of leaf photosynthetic capacity among Salix species. In panels a-c, path analyses test the direct and indirect relationships between biometric trait, chemical and photosynthetic processes to explain A_{sat} variation of three Salix species co-occurring in the glacier Qarlikturvik valley of Bylot Island. The original path model is presented in Figure 1. Positive and negative causal relationships are represented by full and dashed simple arrows, respectively. Covarying partial relationships are represented by double arrows. The path coefficients on simple arrows are simple standardized regression coefficients and the ones on double arrows resulted from Pearson correlation. The goodness-of-fit is given with the overall model P-value and the Fisher C test. The arrow thickness is weighted by the standardized estimates of regression coefficients. In panels d-e, conditional analyses of variance testing the differences in photosynthetic nitrogen-use efficiency (PNUE = A_{sat}/N_{area}) and instantaneous water-use efficiency (iWUE = $A_{sat}/(1.6 \cdot g_{sc})$) among the three Salix species. Conditional relationships were fitted using generalized regression models considering sampling date and site as random factors and using gamma distribution for both PNUE and iWUE.

Supplementary materials

Carboxylation capacity is the main limitation of carbon assimilation in High-Arctic salix shrubs

Jennifer Paillassa, Steeve Pepin, Gilbert Ethier, Laurent J. Lamarque, Lucas Deschamps, Vincent Maire

The supplementary materials include:

Figure S1: Representative A-C_i curves for our three *Salix* species.

Figure S2: Coordination of biochemical limitations to leaf photosynthesis.

Table S1: Report of J_{max}-Vc_{max} interaction values from the literature

Figure S3: Conditional relationships explaining the variation of g_{sc}, g_m and Vc_{max} as a function of P_{area}, N_{area} and LMA.

Table S2: Statistics from a mixed regression model testing the influence of leaf dry matter content, leaf thickness and leaf nitrogen content on the mesophyll conductance.

Figure S4: Conditional relationships explaining the variation of g_m as a function of leaf dry matter content, leaf thickness and leaf nitrogen content.

Figure S5: Fraction of leaf nitrogen into Rubisco (fLNR) in relation to LMA.

Figure S6: Photosynthetic nitrogen use efficiency variation in relation to intercellular and chloroplastic CO_2 concentrations.

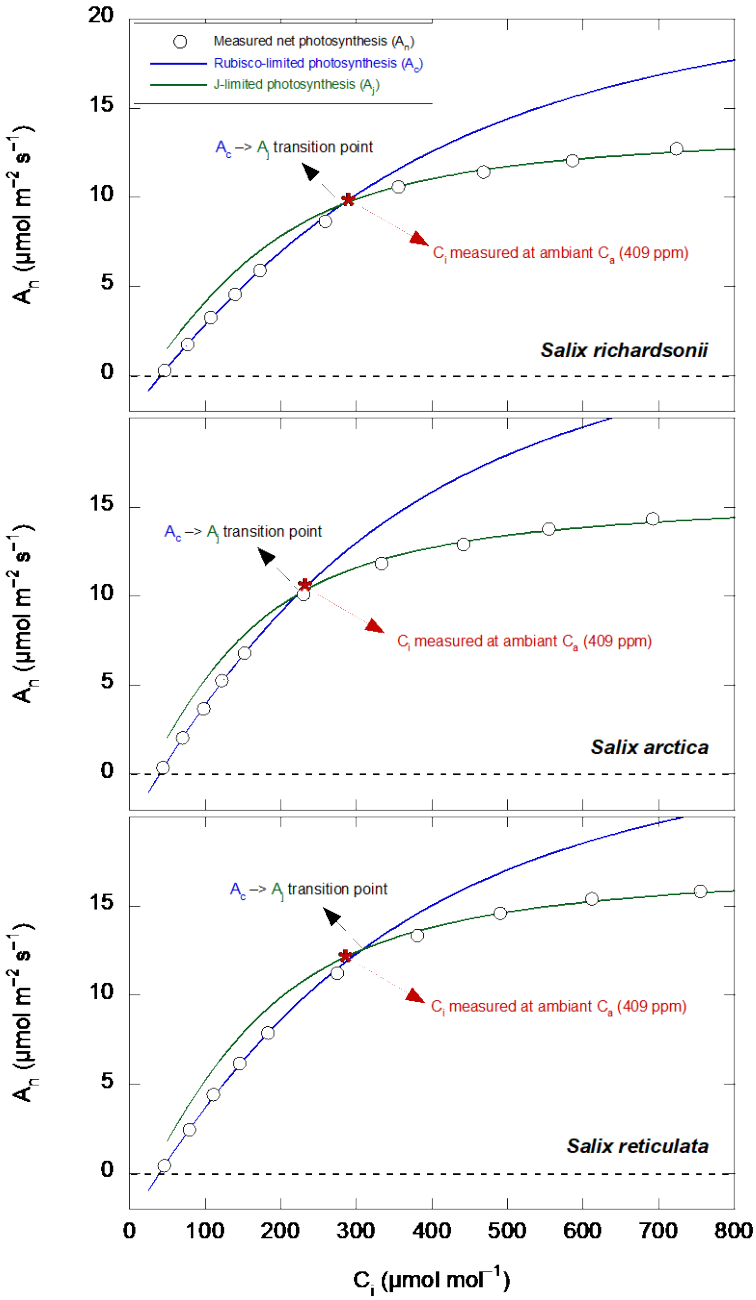

Figure S1: Representative A-C_i curves for our three *Salix* species. The intercellular concentration of CO_2 (C_i) at the transition point between A_c (Rubisco-limited photosynthesis) and A_j (J-limited photosynthesis) is indicated by a black arrow at the crossing of the two curves whereas the C_i value measured at ambient CO_2 conditions (C_a = 409 ppm) is indicated by a red asterisk.

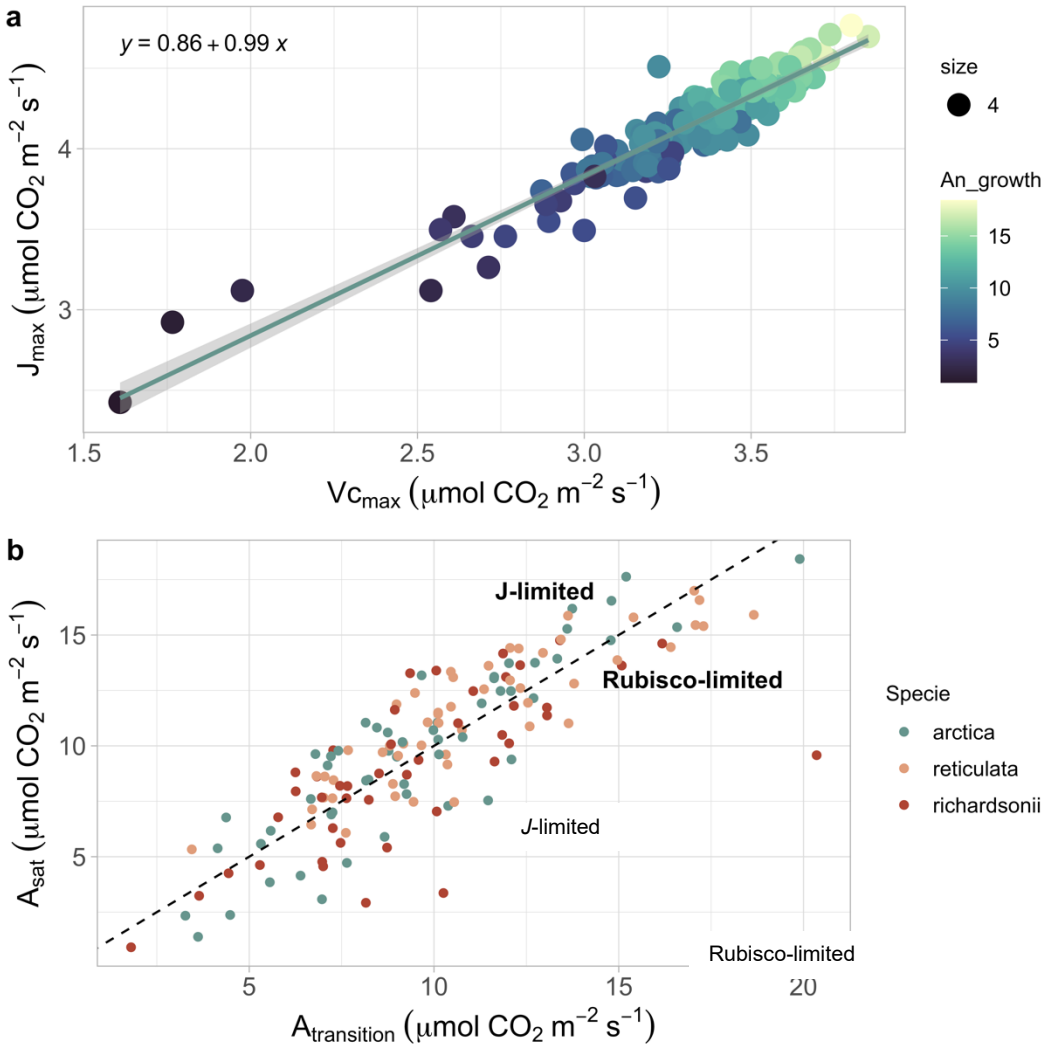

Figure S2: Coordination of biochemical limitations to leaf photosynthesis in the three Salix species co-occurring in the Qarlikturvik valley of Bylot Island (Nunavut)**.** Panel a shows the relationship between Vc_{max} and J_{max}. Panel b shows the relationship between the light-saturated net photosynthetic rate (A_{sat}) at ambient CO_2 concentration (C_a = 409 ppm) and the net assimilation rate at the transition point between the Rubisco-limited and *J*-limited portions of the A-C_i response curves (n = 162 Salix individuals). Dashed line equation: A_{sat} = 0.9928 x $A_{transition}$ (R^2 = 0.96).

Table S1: Report of J_{max}-Vc_{max} interaction values from the literature. The table shows the intercepts and slope of the relationship between J_{max} and Vc_{max} found in the literature to compare to our results. To do the comparison between studies, we transformed Vc_{max} and J_{max} values using a $\log_{10}$.

Studies reporting Jmax ~ Vcmax	**intercept**	**Slope**
Walker et al. 2014	1.010	0.890
TRY/Kattge (2007)	1.668	0.750
Wullschlleger (1993)	1.425	0.837
This study	0.857	0.991

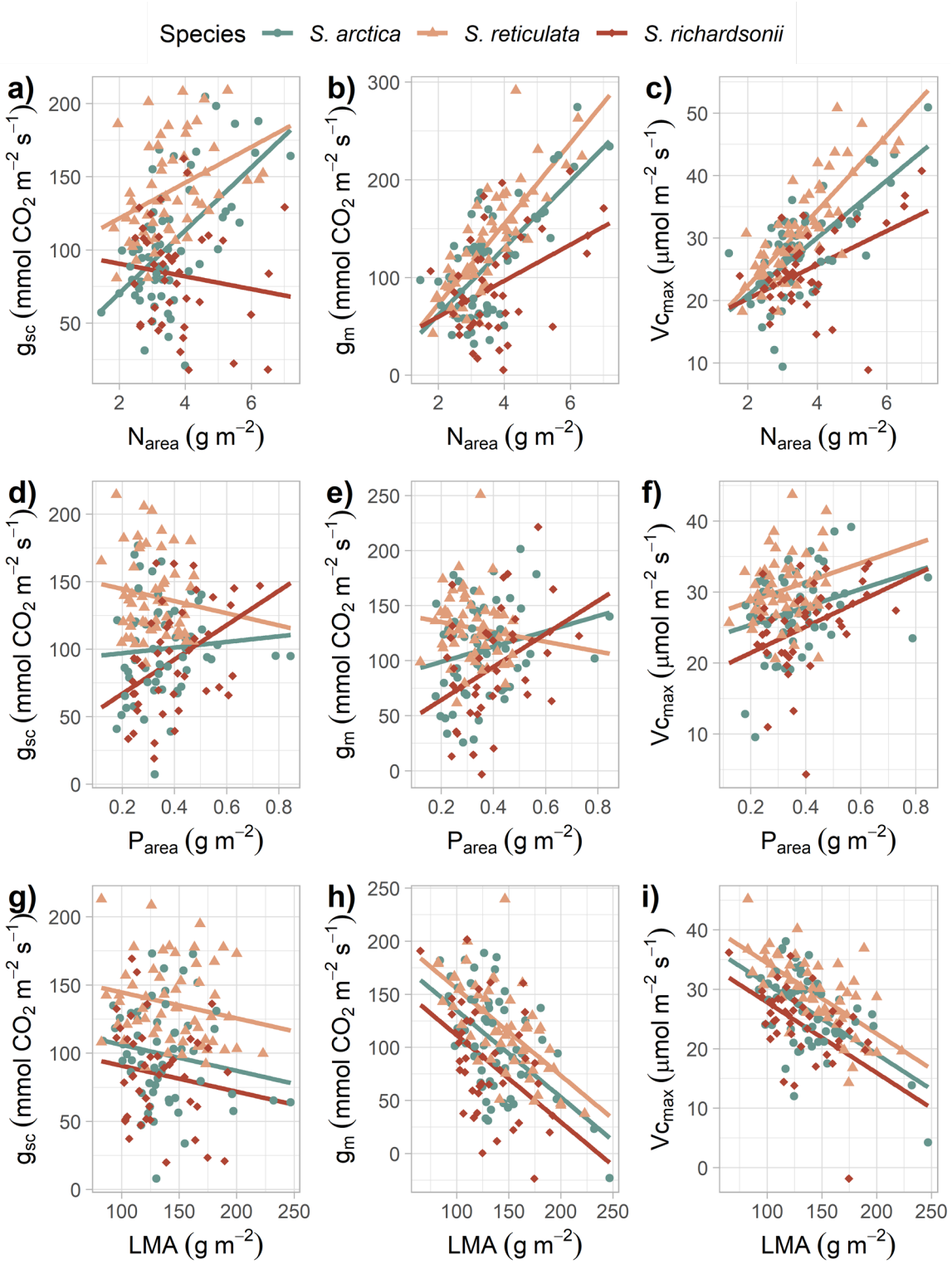

Figure S3: Conditional relationships explaining the variation of g_{sc}, g_m and Vc_{max} as a function of leaf P concentration per unit area, leaf N concentration per unit area and LMA of three Arctic Salix species. Conditional relationships were fitted using generalized regression models of Table 3, where sampling date and site were used as random factors. We considered significant explicative variables only.

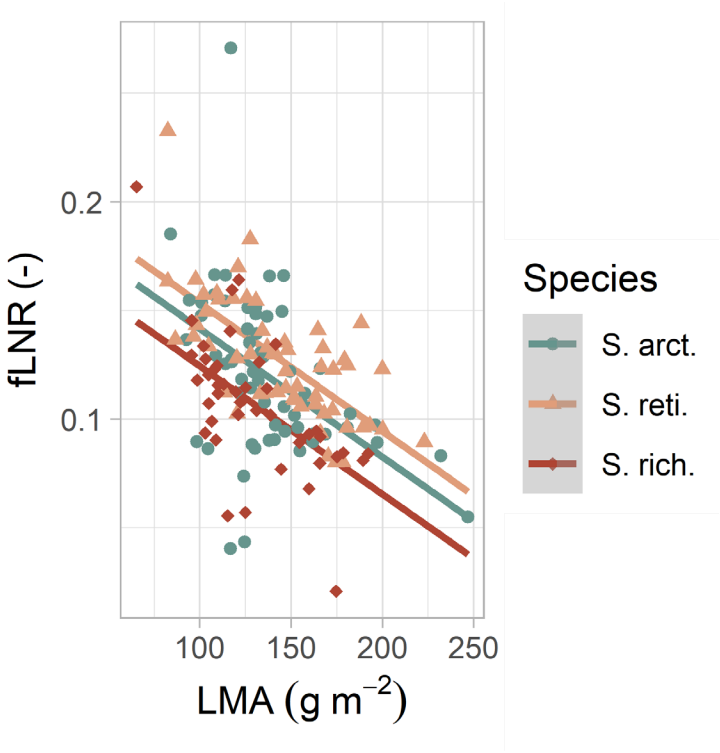

Figure S4: Fraction of leaf nitrogen into Rubisco (fLNR) (Luo et al., 2021) in relation to leaf mass area (LMA) Species were *S. arctica*, *S. reticulata* and *S. richardsonii*. The relationship was from a mixed regression model considering site and date as random factors. fLNR = 0.201 + $5.90 \cdot 10^{-4} \cdot$LMA + 0·(*S. arctica*) + 0.012·(*S. reticulata*) - 0.017·(*S. richardsonii*), (r_m^2 = 0.29, r_c^2 = 0.43, *P-value* < 0.001).

Table S2: Statistics from a mixed regression model testing the influence of leaf dry matter content (LDMC, g g^{-1}), leaf thickness (LT, µm) and leaf nitrogen content (N_{area}, gN m^{-2}) on the mesophyll conductance (g_m, mmol m^{-2} s^{-1}). We considered site and sampling date as random factors, and LDMC, LT, N_{area}, and species as fixed factors. We used the Gaussian family distribution for all dependent variables and n = 157.

Model factors	DF	Estimate	F-value	P-value
Species	2	*S. reticulata* = 16.8 ± 9.3 *S. richardsonii* = -23.1 ± 9.7	6.6	ns ***
N_{area}	1	28.6 ± 7.5	14.5	***
LT	1	-0.229 ± 0.111	4.2	*
LDMC	1	-220.0 ± 58.8	5.3	*
Overall		r^2_m = 0.14; r^2_c = 0.40	AICc = 1394	

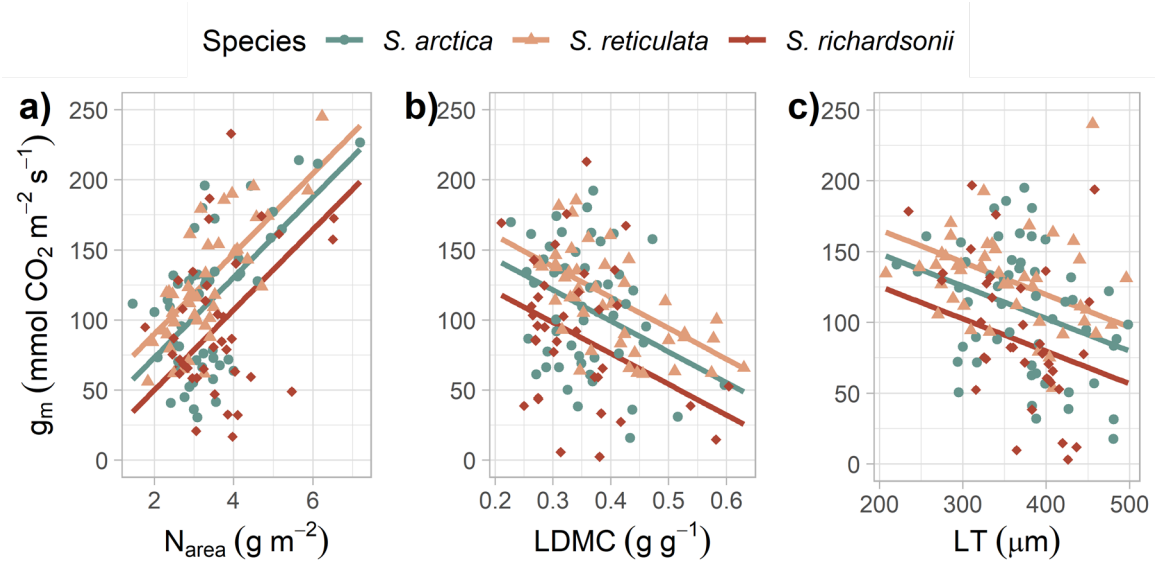

Figure S5: Conditional relationships explaining the variation of g_m as a function of leaf dry matter content (LDMC), leaf thickness (LT) and leaf nitrogen content (N_{area}) and Arctic Salix species. Conditional relationships were fitted using generalized regression models of Table S2, where sampling date and site were used as random factors. We considered significant explicative variables only.

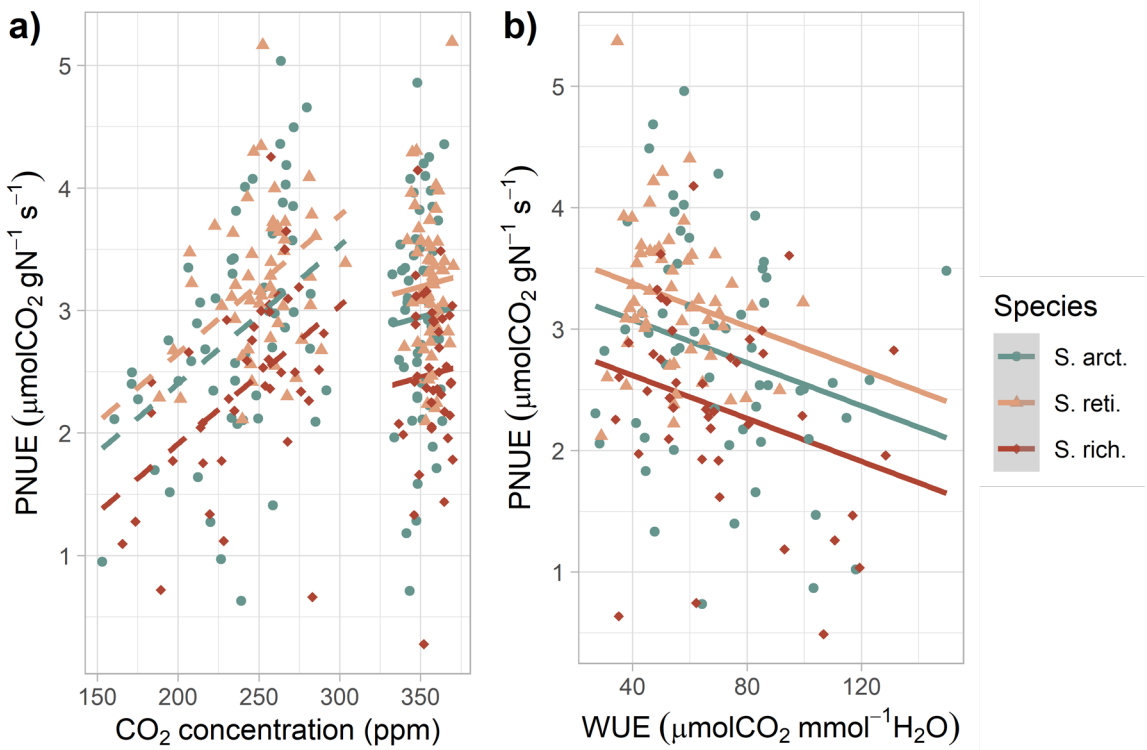

Figure S6: Photosynthetic nitrogen use efficiency variation of three Salix species (*S. arctica*, *S. reticulata* and *S. richardsonii*) in relation to (a) intercellular (solid line) and chloroplastic CO_2 (dashed line) concentration, and to (b) intrinsic water use efficiency (A/g_s). The relationships were from mixed regression models considering site and date as random factors. The regression details were: (a) PNUE = -1.14 + 0.011 · C_c + 0.004 · C_i (r_m^2 = 0.24, r_c^2 = 0.56, *P-value* < 0.001); (b) PNUE = 3.43 - 0.0088 · WUE (r_m^2 = 0.16, r_c^2 = 0.38, *P-value* < 0.001)**.**